PHYSICAL, CHEMICAL AND RHEOLOGICAL STUDIES OF THE HEN'S EGG

by

MARVIN ARTHUR TUNG

B.S.A., University of British Columbia, 1960

M.S.A., University of British Columbia, 1967

A THESIS SUBMITTED IN PARTIAL FULFILMENT OF

THE REQUIREMENTS FOR THE DEGREE OF

DOCTOR OF PHILOSOPHY

in the Department

of

Food Science

We accept this thesis as conforming to the

required standard

THE UNIVERSITY OF BRITISH COLUMBIA

August, 1970

In presenting this thesis in partial fulfilment of the requirements for an advanced degree at the University of British Columbia, I agree that the Library shall make it freely available for reference and study. I further agree that permission for extensive copying of this thesis for scholarly purposes may be granted by the Head of my Department or by his representatives. It is understood that copying or publication of this thesis for financial gain shall not be allowed without my written permission.

MARVIN A. TUNG

Department of Food Science
The University of British Columbia,
Vancouver 8, Canada
Date Sept 11, 1970

ABSTRACT

A three-part investigation is described in which hardness at regular intervals across the thickness of egg shells is measured and related to chemical composition at similar positions in the same shells; egg shell membranes are viewed by electron microscopy to compare the structure of inner and outer layers; and rheology of egg albumen is studied using a rotational viscometer.

Microindentation tests of 27 egg shells reveal a maximum hardness at the outer surface, intermediate hardness at the inner surface and a minimum hardness midway across the thickness of the shell. Electron probe microanalyses indicate a gradual linear increase in calcium toward the inner shell surface. Magnesium and phosphorus are a maximum at the outer surface and follow quadratic and exponential gradients respectively across the egg shell thickness. Hardness gradients, composition gradients and the hardness-composition relationships change from shell to shell. For individual egg shells, an average of 91 percent of the variation in hardness is accounted for by variations in chemical composition. In pooled data of 27 shells, 48 percent of hardness variance is associated with composition changes; whereas 81 percent may be attributed to variations in composition and position in the shell.

Electron microscopical study and measurement of four egg shell membranes show that the structures consist of an open

network of fibers built up in layers parallel to the membrane surfaces. Two regions are evident in transverse section. The outer membrane is three times the thickness of the inner membrane and the combined dimension is about 100 microns. Each fiber has a central core encased by a granular mantle. For the outer membrane, fiber core diameters are significantly greater and fibers usually occupy a larger percentage of membrane volume than is the case for inner membranes. The inside surface of the inner membrane is lined by a 0.1 micron layer of material similar to the fiber mantle. Egg shell membrane structure is discussed in relation to microbial penetration.

Viscous behavior of egg albumen is described at 10, 20, 30 and 40°C between shear rates of 220 and 3140 sec^{-1}. Egg albumen is a time-dependent pseudoplastic fluid. Apparent-viscosity decay at constant shear rate is partially recoverable between 32 hour tests and is affected by the temperature and shear rate used. Flow behavior is accurately described by the power-law and Ellis models. Shear history strongly influences flow behavior with higher shear rates resulting in greater pseudoplasticity and sensitivity to temperature effects.

TABLE OF CONTENTS

	Page
LIST OF TABLES	ix
LIST OF FIGURES	xi
ACKNOWLEDGMENTS	xiv
INTRODUCTION	1
CHAPTER I. HARDNESS AND COMPOSITION OF THE SHELL	2
REVIEW OF THE LITERATURE	3
EXPERIMENTAL METHODS	4
Measurement of Shell Hardness	4
Preparation of specimens	4
Test procedure	5
Measurement of Average Chemical Composition	6
Calcium and magnesium determination	6
Phosphorus determination	8
Estimation of organic content	8
Electron Probe Microanalyses	9
Preparation of specimens	9
Electron beam scans	9
Step-scans across the shell	10
Reduction of microprobe data	11
Conversion of microprobe data to composition	12
Relation of Hardness to Chemical Composition	17

Page

RESULTS AND DISCUSSION 17

Results of Hardness Tests 17

Results of Chemical Composition by Solution Methods 23

Results of Electron Probe Microanalyses 23

Electron beam scans 23

Step-scans across the shell 27

Comparison of Chemical Analyses by Solution Methods and the Electron Microprobe 34

Relation of Hardness to Chemical Composition 35

SUMMARY AND CONCLUSIONS 40

CHAPTER II. STRUCTURE OF EGG SHELL MEMBRANES 42

REVIEW OF THE LITERATURE 42

EXPERIMENTAL METHODS 44

Preparation of Specimens 44

Examination by Electron Microscopy 45

Measurement of Fiber Dimensions 46

Analysis of Data 46

RESULTS AND DISCUSSION 49

Qualitative Observations on Membrane Structure 52

Results of Measurements of Membrane Structure 52

Membrane thickness and fiber area density 52

Mean values of fiber measurements 54

Variation in fiber measurements across the membrane 56

Page

SUMMARY AND CONCLUSIONS 60

CHAPTER III. RHEOLOGY OF EGG ALBUMEN 62

REVIEW OF THE LITERATURE 62

EXPERIMENTAL METHODS 63

Preparation of Samples 63

Test Procedures 64

Rheological Models 65

Models of time-dependent behavior 65

Models of flow-behavior 67

Temperature Effects on Flow Behavior 68

Temperature dependence of flow parameters 68

Temperature dependence of viscosity 69

Statistical Methods Used in Data Analysis 69

RESULTS AND DISCUSSION 70

Sample Quality 70

Results of Time Dependence Tests 70

Recovery of apparent viscosity after storage 70

Effect of shear rate on apparent-viscosity decay 72

Effect of temperature on apparent-viscosity decay 72

Results of Flow-Behavior Tests 76

Effect of storage on flow behavior 76

Effect of maximum shear rate on flow behavior 76

Page

The power-law model of flow behavior 78

The Ellis model of flow behavior 81

Results for Temperature Effect on Flow Behavior 81

Effect of temperature on flow-behavior parameters 81

Effect of temperature on apparent viscosity 84

SUMMARY AND CONCLUSIONS 90

LITERATURE CITED 91

LIST OF TABLES

Table		Page
I	Atomic Absorption Spectrophotometer Operating Conditions	7
II	Diamond Pyramid Hardness (Kg/mm^2) across the Thickness of Egg Shells	20
III	Analysis of Variance in Hardness Data	22
IV	Percentage Composition of Egg Shells by Solution Methods	24
V	Average Percentage Composition of Egg Shells by Electron Probe Microanalysis	28
VI	Average Percentage Composition at Ten Shell Levels in 27 Egg Shells by Electron Probe Microanalysis	29
VII	F-Ratios from Analyses of the Variance in Composition of Egg Shells by Electron Probe Microanalysis	33
VIII	Multiple Curvilinear Regressions of Hardness on Composition - Pooled Basis (n = 270)	36
IX	Coefficients of Multiple Determination for Regressions of Hardness on Composition - Individual Shell Basis (n = 10)	37
X	Multiple Curvilinear Regressions of Hardness on Composition and Shell Level - Pooled Basis (n = 270)	39
XI	Thickness and Fiber Area Density of Egg Shell Membranes	53
XII	Mean Values of Egg Shell Membrane Measurements	55
XIII	Apparent-Viscosity Decay Curves for NV Spindle	74
XIV	Apparent-Viscosity Decay Curves for MV1 Spindle	75

Table		Page
XV	Power-Law Flow-Behavior Curves for Egg Albumen	80
XVI	Ellis Model Flow-Behavior Curves for Egg Albumen	82
XVII	Temperature Dependence of Power-Law Flow-Behavior Parameters	85
XVIII	Temperature Dependence of Ellis Model Flow-Behavior Parameters	85
XIX	Temperature Dependence of Apparent Viscosity Using Shear Rate as a Parameter	89

LIST OF FIGURES

Figure		Page
1	Hardness in 27 egg shells. The mean ± one standard deviation is shown at each shell level.	18
2	Calcium K_α electron beam scan at the outer edge of an egg shell. (790X)	25
3	Magnesium K_α electron beam scan at the outer edge of an egg shell. (790X)	25
4	Phosphorus K_α electron beam scan at the outer edge of an egg shell. (790X)	26
5	Magnesium K_α electron beam scan at the inner edge of an egg shell. (790X)	26
6	CaO content of 27 egg shells. The mean ± one standard deviation is shown at each shell level.	30
7	MgO content of 27 egg shells. The mean ± one standard deviation is shown at each shell level.	30
8	P_2O_5 content of 27 shells. The mean ± one standard deviation is shown at each shell level.	32
9	Schematic diagram of an oblique section through an egg shell membrane fiber to illustrate the dimensions measured.	47
10	WL1 outer egg shell membrane (6660X).	50
11	WL2 inner egg shell membrane (6660X).	50
12	NH1 outer egg shell membrane (7050X).	51
13	NH1 inner egg shell membrane (11200X).	51
14	Fiber core diameters for membrane WL1. The mean and standard deviation at each level are shown.	57

Figure		Page
15	Fiber core diameters for membrane WL2. The mean and standard deviation at each level are shown.	57
16	Fiber core diameters for membrane NH1. The mean and standard deviation at each level are shown.	58
17	Fiber core diameters for membrane NH2. The mean and standard deviation at each level are shown.	58
18	Average fiber mantle thickness for membranes WL1 and WL2.	59
19	Average fiber mantle thickness for membranes NH1 and NH2.	59
20	Apparent-viscosity decay in egg albumen tested before and after 32 hours storage. Tests at 10°C and 3140 sec^{-1} shear rate.	71
21	Apparent-viscosity decay in egg albumen at 10°C with shear rates of 1570 and 3140 sec^{-1}.	71
22	Apparent-viscosity decay curves at 10, 20, 30 and 40°C - NV spindle.	73
23	Apparent-viscosity decay curves at 10, 20, 30 and 40°C - MV1 spindle.	73
24	Flow behavior of egg albumen samples tested before and after 32 hours storage. Tests at 10°C with NV spindle.	77
25	Flow behavior of egg albumen at 10°C for maximum shear rates of 1570 and 3140 sec^{-1}.	77
26	Flow-behavior curves for egg albumen at 10, 20, 30 and 40°C - NV and MV1 spindles.	79
27	Temperature dependence of the power law parameter m.	83
28	Temperature dependence of the power law parameter n.	83

Figure		Page
29	Temperature dependence of the Ellis parameter α.	86
30	Temperature dependence of the Ellis parameter $\tau_{1/2}$.	86
31	Temperature dependence of the Ellis parameter η_o.	87

ACKNOWLEDGEMENTS

The author extends his appreciation for assistance by Dr. J.F. Richards, Food Science Department; Professor L.M. Staley and Professor E.L. Watson, Agricultural Engineering Department; Dr. J.B. Farmer, Chemistry Department; Dr. J. Biely, Poultry Science Department and Dr. L.C. Brown, Metallurgy Department, the University of British Columbia.

The writer is grateful for the use of an electron probe and hardness tester in the Metallurgy Department, an electron microscope in the Biology Department and a viscometer in the Agricultural Engineering Department.

This research was financed by the National Research Council of Canada.

INTRODUCTION

The hen's egg is an important food in most parts of the world for which the annual production is in excess of 300 billion eggs. Preservation of the edible portion of the egg is aided by a leathery membrane and calcareous shell encasement that minimizes chemical degradation and microbial invasion. The shell also provides a relatively durable, convenient unit for handling the product. Physical and chemical studies of egg shells and their membranes are fundamental to explaining their roles in maintaining egg quality.

Large quantities of liquid egg are processed commercially after removing the shell and membranes. Operations include separating, pumping, heat exchanging, mixing and spray drying -- all of which are governed by the viscous nature of the fluids. Rheological studies on egg constituents would provide data useful in the design and evaluation of liquid egg handling equipment.

This thesis describes a three-part investigation of the hen's egg in which hardness at regular intervals across the thickness of egg shells was measured and related to chemical composition at similar positions in the same shells; egg shell membranes were viewed by electron microscopy in order to compare the structure of inner and outer layers; and rheology of egg albumen was studied using a rotational viscometer.

CHAPTER I. HARDNESS AND COMPOSITION OF THE SHELL

Most eggs are marketed in their shells; thus, damaged shells are undesirable and present a potential public health hazard. Losses due to broken and cracked shells are estimated at over five percent of the retail product value. Egg shell strength has received considerable study in the past decade (W3, H3, T9)* as a result of its economic importance.

Shell hardness is of interest because hardness of crystalline materials is closely related to strength (T1) and may be used as a measure of mechanical properties (M3). Since microindentation hardness tests permit measurements on small amounts of material and on brittle specimens, egg shell hardness may be tested by this method.

Egg shells are mainly calcium carbonate in the calcite form (T2) with small amounts of impurities such as magnesium and phosphorus. These elements are of interest in relation to hardness because magnesium substitution for calcium in the calcite lattice results in a harder crystal and furthermore, calcium phosphate is harder than calcium carbonate. The purpose of this study was to measure hardness and chemical composition point-by-point across the thickness of several egg shells and to identify the relation between these two characteristics.

---

* Alphanumeric characters in parentheses are in reference to the literature cited.

REVIEW OF THE LITERATURE

Brooks and Hale (B6) measured the hardness of twenty egg shells using radial sections and reported a linear gradient of hardness decreasing toward the inner surface. They tested hardness at shell levels 0.25, 0.50, and 0.75 (shell levels 0.0 and 1.0 correspond to outer and inner surfaces respectively) because brittleness of the material prevented measurements near the unsupported edge of the shells.

In a preliminary study by Tung (T3), hardness was tested in radial and tangential sections of egg shell. The use of tangential sections permitted hardness determinations between shell levels 0.02 and 0.90. Egg shells were found to be hardest near the outer surface, of intermediate hardness near the inner surface and softest midway between. Gradients of hardness between shell levels 0.20 and 0.70 were found to be similar for radial and tangential tests on the same shells.

Variation in magnesium content in the shell was reported by Brooks (B7) and later by Itoh and Hatano (I1) who also noted an unequal distribution of phosphorus. The method used in each case was to progressively dissolve the shell in five approximately equal layers and analyze the resulting solutions. Magnesium to calcium ratios were greatest near the outer surface and decreased to a minimum near shell level 0.70. Gradients were semi-logarithmic for the data of Brooks and linear for Itoh and Hatano. The phosphorus to calcium ratio was a maximum in the outer layer of the shell and essentially constant throughout the remaining portions.

A recent advance in analytical chemistry is the electron microprobe (B3, B8, K2, O1) which can be used to measure the chemical composition of a few cubic microns of solid material and is thus well suited to detecting composition differences in crystalline substances. The use of hardness gradient measurement techniques as described by Tung (T3) in combination with electron probe analysis should provide the point-by-point comparison of hardness and chemical composition required for this study.

EXPERIMENTAL METHODS

Measurement of Shell Hardness

Preparation of specimens

Three eggs from each of nine Single-Comb White Leghorn pullets provided a total of 27 shells for hardness tests. A line was drawn on the equator of each egg and its diameter measured prior to breaking the egg and removing shell membranes by boiling in 0.6 M sodium hydroxide. The shell was then thoroughly rinsed in water and dried in an oven at 80°C. Thickness at the shell equator was measured. A sample of the shell was mounted in epoxy (Epon 828 + 10% diethylenetriamine by weight) and the convex surface ground away to expose a tangential section at the shell equator. The surface was polished with a series of emery papers and aluminum oxide lapidary wheels before measuring the length

of the exposed section in the direction of the egg equator. Since the egg is essentially circular in the plane of its equator, the shell diameter and thickness may be used to locate any desired shell level on the exposed tangential surface (T4) with an estimated error of less than 2 percent.

Test procedure

Hardness was measured using a Tukon microindentation hardness tester (M3) equipped with a square-based diamond pyramid indenter under 100 g load. The indenter was forced into the polished surface of the shell and the diagonal lengths of the resulting indentation were measured with an ocular micrometer on the testing machine. Diamond pyramid hardness was calculated from the average diagonal length using the equation

$$H_{DP} = \frac{1.8544\ L}{d^2} \qquad [1]$$

where H_{DP} = diamond pyramid hardness, kg/mm^2

L = load on indenter, kg

d = average diagonal length, mm.

Hardness measurements were standardized during each series of tests by means of a calibrated reference block.

Three tests were made at shell levels 0.02, 0.10, 0.20, 0.30, 0.40 and 0.50 starting from one edge of the exposed section along a narrow strip containing the equator. A duplicate set of tests was made starting at the opposite edge of the section so that the average of six indentations

was used to calculate hardness at each shell level. After tests were made from levels 0.02 to 0.50, the original test block was cast in epoxy and ground away to expose a tangential section from the concave surface on which hardness was measured at levels 0.50, 0.60, 0.70, 0.80 and 0.90 in a similar manner. Overlapping tests at shell level 0.50 provided 12 indentations from which hardness at that level was calculated.

Measurement of Average Chemical Composition

Calcium and magnesium determination

For each of the 27 egg shells, a sample was powdered using a mortar and pestle and 0.3000 g weighed into a 100 ml beaker. Three ml of concentrated HNO_3, 3 ml of concentrated HCl and 9 ml of water were added. The beaker was covered with a watch glass and boiled for ten minutes to dissolve the sample. The solution was filtered into a 500 ml volumetric flask and the filter paper was washed with 20 ml of 0.5 N HCl. Twenty ml of 5 percent lanthanum chloride solution was added and the flask filled to the mark with water. The resulting solution was anlyzed for magnesium and a portion of it diluted to six times its volume and analyzed for calcium. The purpose of the lanthanum was to overcome possible interferences by other ions in the analyzed solutions (El). Chemicals were of analytical grade and distilled deionized water was used in all preparations.

A Unicam SP 90 atomic absorption spectrophotometer equipped with a strip chart recorder was used in the analyses for magnesium and calcium. The instrument was fitted with a 10 cm acetylene burner operated to give a fuel-rich luminous flame under the conditions specified in Table I.

TABLE I. ATOMIC ABSORPTION SPECTROPHOTOMETER OPERATING CONDITIONS

	Calcium	Magnesium
Wavelength, nm	422.7	285.2
Slitwidth, nm	0.08	0.1
Lamp current, mA	12	4
Acetylene pressure, kg/cm^2	0.7	0.7
Acetylene flow rate, ml/min	1500	1500
Air pressure, kg/cm^2	2.1	2.1
Air flow rate, l/min	5	5

A series of solutions up to 4.0 mg/l for magnesium and 40.0 mg/l for calcium was prepared for the spectrophotometer calibration. The standard curves were concave to the absorbance axes; hence, the least squares quadratic fit of absorbance to concentration formed the calibration curve in each series of tests. Percentage compositions of calcium and magnesium in the original samples were based on the

calibration curves, dilution factors and original sample weights.

Phosphorus determination

Powdered samples of each shell were placed in weighed crucibles, dried overnight at 105°C and reweighed. Specimens were then heated in an oven at 1000°C to remove organic matter, and weighed again. Duplicate 0.1200 g portions of the residue from each egg shell were placed in 250 ml Erlenmeyer flasks, 20 ml of 60% perchloric acid added and the mixture boiled for 10 minutes to digest the sample. The solutions were made up to 250 ml with water in volumetric flasks.

Fifty ml portions of the acid solutions were transferred to 100 ml volumetric flasks to be analyzed for phosphorus (B4). Five ml of 0.1 M sodium molybdate in 5.0 M sulfuric acid were added along with 2.0 ml of 0.012 M hydrazine sulfate and the flasks filled to volume with water. The flasks were immersed in boiling water for 10 minutes, then cooled rapidly. Absorbance at 830 nm was read in a Spectronic 20 spectrophotometer for the unknown and standard phosphate solutions. Values of percentage phosphorus in the egg shell samples were calculated from the calibration curves, dilution factors and initial sample weights.

Estimation of organic content

Egg shells are known to possess an organic matrix

(S2, T2) that extends through the calcite crystals. An estimate of the organic content of the shell may be derived from the weight loss when heated to 1000°C. Calcium and magnesium, present as carbonates, decompose to their oxides while phosphorus is stable as phosphate; thus, weight loss due to carbon dioxide production may be calculated from calcium and magnesium composition. The remaining decrement was attributed to oxidation of organic matter since other constituents do not exceed trace amounts (R3). It should be pointed out that this method provided an estimate of organic content subject to inaccuracy due to the combined uncertainties in measurement of magnesium, calcium and phosphorus and the disregard of possible trace elements.

Electron Probe Microanalyses

Preparation of specimens

Samples from the equators of all 27 experimental shells were cast in epoxy along with standard specimens for calcium, magnesium and phosphorus. The epoxy blocks were polished to expose radial sections of shell with a 0.05 micron finish, then a thin coating of carbon was vacuum evaporated onto the surface of the block to render it conductive. The standards were calcite for calcium, magnesium carbonate for magnesium and fluorapatite [$Ca_5(PO_4)_3F$] for phosphorus.

Electron beam scans

Composition of crystalline materials may differ

from crystal to crystal boundaries, hence preliminary tests were conducted to determine whether calcium, magnesium and phosphorus occur uniformly within the shell.

The U.B.C. Department of Metallurgy electron microprobe (JEOLCo Model JXA-3A with 20° takeoff angle) was used to obtain qualitative information on the distribution of calcium, magnesium and phosphorus in the shell. Calcium K_α X-radiation was analyzed with a quartz crystal spectrometer whereas magnesium K_α and phosphorus K_α lines used mica crystals. Analysis of phosphorus in the presence of calcium was complicated by interference of second order Ca K_β (3.090 Å) radiation with P K_α (6.154 Å) because both lines are diffracted at the same spectrometer setting. Since the two lines have different energies, pulse height analysis was used to exclude the interfering calcium signal.

The probe was operated at 15 kV accelerating potential with 0.05 μA sample current normalized on brass and a minimal spot size. Electron beam scans were made near both edges of one egg shell in areas that included several crystal boundaries. Absorbed electron images were recorded to aid in identifying the regions scanned.

Step-scans across the shell

Five-micron step-scans at 10 second counts were run on radial sections of 27 egg shells to measure calcium, magnesium and phosphorus content point-by-point across the

thickness of each shell. Probe conditions were 15 kV accelerating potential, 0.05 μA sample current normalized on brass and a spot diameter of about 5 microns. Spots were tested on each standard at one-hour intervals for signal calibration and drift evaluation.

Reduction of microprobe data

The shell level corresponding to each analyzed spot was computed and the raw X-ray intensity data divided into ten portions such that each level previously tested for hardness was spanned by a set of microprobe data. For example:

$X = 0.02$, $0.0 < X < 0.05$; $X = 0.10$, $0.05 < X < 0.15$,..., $X = 0.90$, $0.85 < X < 0.95$ where X is the shell level. To evaluate calcium, magnesium and phosphorus X-ray intensities at the ten shell levels of interest, the least squares simple linear regressions of intensity on shell level were computed for the three elements in each range and the equations solved for the desired shell level. Thus, calcium, magnesium and phosphorus X-ray intensities at shell levels 0.02, 0.10, 0.20, ..., 0.90 were obtained. This procedure serves to smooth the microprobe data and preserve the effect of composition gradients where the data are not symmetrical about the shell level of interest. The amount of data is also reduced to correspond with the hardness information available.

Conversion of microprobe data to composition

Drift due to fluctuations in the instrument electronic components was evaluated from the periodic tests on standards and a linear drift correction was applied to the counting rates of the standards associated with the data of each egg shell. Thus, drift was assumed to be linear between tests of successive shells and was neglected during the analysis of each shell. This procedure was judged to be satisfactory since the average drift correction from shell to shell was less than 0.5 percent.

The calcium weight fraction for each shell level was calculated by assuming direct proportionality between X-ray intensities and concentrations in both the calcite and the egg shell. This method is simple, yet suitable for the present analysis because of the close similarity between the standard and unknown.

Magnesium and phosphorus X-ray intensity data for the standards and unknowns were modified by a number of correction procedures (G2, S6). The influence of detector dead-time on all signals was corrected using

$$N_2 = \frac{N_1}{(1-N_1 t)} \qquad [2]$$

where N_1 = observed count rate

N_2 = true count rate and

t = detector dead-time.

The background intensity was then considered. That is,

$$N_3 = N_2 - B \qquad [3]$$

where N_3 = corrected count rate and

B = background count rate.

Apparent weight concentrations of the specimens were calculated by direct proportionality between X-ray intensities and concentrations for standards and unknowns.

$$C_1 = C_s \frac{(N_3)_u}{(N_3)_s} \qquad [4]$$

where C_s = weight concentration of standard

C_1 = apparent weight concentration

u and s refer to unknown (egg shell) and standard. The assumption of proportionality is inaccurate when samples and standard are dissimilar because of the differing effects of atomic number, mass absorption and fluorescence on the respective X-ray intensities.

Microprobe correction procedures for atomic number, absorption and fluorescence require an estimate of specimen composition. However, when the corrections have been applied, a better estimate of composition is available which may be used to recalculate the correction factors. Thus the cycle is repeated until no further improvement results. Magnesium and phosphorus apparent concentrations were taken from equation [4] and calcium concentration from the calculation described earlier. Carbon and oxygen of the crystalline

phase were computed on the assumption that calcium carbonate, magnesium carbonate and calcium phosphate were the only inorganic substances present. The remaining weight of the shell was attributed to the organic matrix which is known to be a protein-acid mucopolysaccharide complex (S2). Composition of the organic material was approximated by 47 percent carbon, 43 percent oxygen and 10 percent nitrogen. With this information the fractional weight composition was calculated for each element present in the shell.

The average atomic number of a test material has an effect on electron backscattering and electron retardation, hence the correction for these two phenomena is termed the atomic number correction (D1). Apparent weight concentration was modified using

$$C_2 = C_1 \frac{\bar{S}_u \bar{R}_s}{\bar{S}_s \bar{R}_u} \qquad [5]$$

where $\bar{R} = \Sigma_i R_i C_i$ [6]

R_i = the backscatter coefficient and

C_i = weight concentration for each element i.

$\bar{S}$ is obtained from

$$\bar{S} = \Sigma_i C_i S_i \qquad [7]$$

where $$S_i = \frac{Z_i}{A_i} \ln \frac{1.166 \times 10^3 \bar{E}}{J_i} \qquad [8]$$

Z_i = atomic number

A_i = atomic weight

J_i = mean ionization potential

$$\bar{E} = \frac{E_o - E_c}{2} \qquad [9]$$

E_o = accelerating potential used and

E_c = excitation potential for the X-ray line studied

A mass absorption correction is required to compensate for partial absorption of X-rays as they travel from point of origin in the sample to the surface. The modified Philibert method (P1, D2) was used in the correction.

$$C_3 = C_2 \frac{f(\chi_s)}{f(\chi_u)} \qquad [10]$$

where C_3 = apparent weight concentration after atomic number and absorption corrections

$$\frac{1}{f(\chi)} = 1 + \frac{1 + 2h}{1 + h}\left[\frac{\chi}{\sigma}\right] + \frac{h}{1 + h}\left[\frac{\chi}{\sigma}\right]^2 \qquad [11]$$

$$h = 1.2 \frac{\Sigma_i N_i A_i}{\left[\Sigma_i N_i Z_i\right]^2} \qquad [12]$$

N_i = atomic concentration

$$\chi = \frac{\mu}{\rho} \text{ cosec } \theta \qquad [13]$$

$\frac{\mu}{\rho}$ = mass absorption coefficient (H5)

θ = takeoff angle

$$\sigma = \frac{2.39 \times 10^5}{E_o^{1.5} - E_c^{1.5}} \qquad [14]$$

In equation [12] weight concentration, C_i, was used to approximate atomic concentration.

Corrections for secondary fluorescence may be needed when an element is analyzed in the presence of characteristic and continuous X-radiation of higher energy than the line of interest. In general, enhancement due to continuous radiation is small and very difficult to evaluate in comparison with that of characteristic radiation (K2). Thus, only fluorescence by characteristic emission lines was considered. Corrections of magnesium and phosphorus intensity ratios for fluorescence by calcium characteristic radiation were calculated with Reed's (R1) simplified procedure and found to be less than 0.1 percent; hence, fluorescence corrections were omitted.

Thus

$$C_4 = C_3 \qquad [15]$$

where C_4 = apparent weight concentration after atomic number, absorption and fluorescence corrections.

At this point the apparent weight concentrations of magnesium and phosphorus were used to reassess specimen composition for the recalculation of atomic number and absorption correction factors. In several separate tests of this procedure with a computer program, there appeared to be no advantage in performing the calculations more than three times.

For the purpose of presenting the total chemical composition, weight fractions were converted to percentage composition as oxides; thus egg shell composition was expressed as percent CaO, MgO, P_2O_5, CO_2 and organic material. It should be emphasized that the possible presence of trace amounts of other elements and the accumulated errors in chemical analyses would be reflected in the organic category because of its method of computation.

Relation of Hardness to Chemical Composition

The electron probe microanalyses provided composition information corresponding to hardness measurements at the same ten shell levels in 27 egg shells; therefore a total of 270 sets of data were available. Relations among the variables were studied by means of analysis of variance, correlation and regression methods. Regressions of hardness on chemical constituents, singly and in combination were computed to assess their relative importance in explaining variation in the dependent variable.

RESULTS AND DISCUSSION

Results of Hardness Tests

Diamond pyramid hardness numbers at ten levels in each of the 27 egg shells appear in Table II. In polynominal fits to the pooled data (n = 270), variation of hardness across the shell thickness (figure 1) is described by the curve

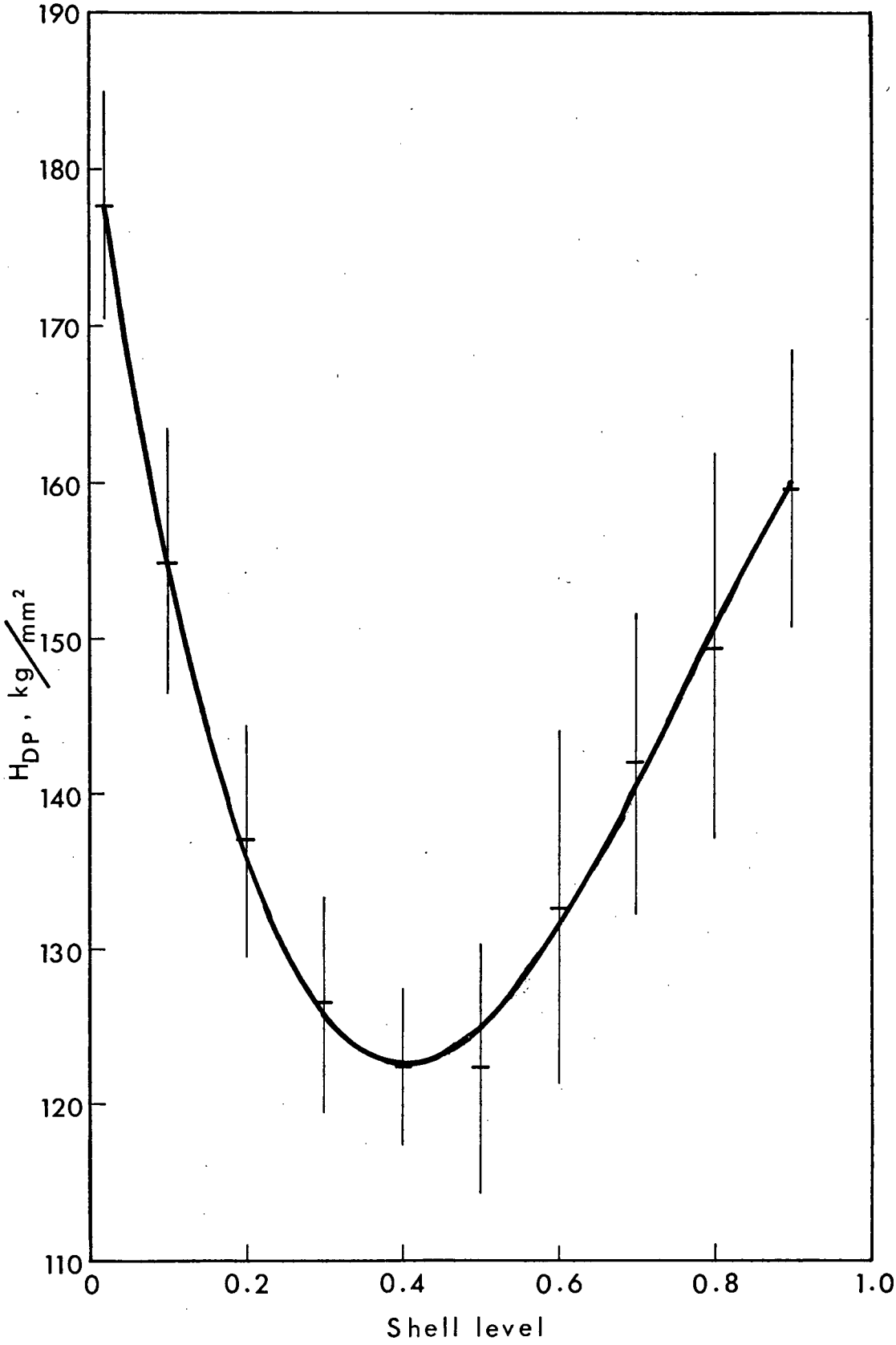

Figure 1. Hardness in 27 egg shells. The mean ± one standard deviation is shown at each shell level.

$$H_{DP} = 184.6 - 350.2X + 591.5X^2 - 259.0X^3 \qquad [16]$$

where H_{DP} = diamond pyramid hardness, Kg/mm^2

X = shell level.

TABLE II. DIAMOND PYRAMID HARDNESS (Kg/mm^2) ACROSS THE THICKNESS OF EGG SHELLS

Shell Number	Bird	Shell level 0.02	0.10	0.20	0.30	0.40	0.50	0.60	0.70	0.80	0.90
1	1	178.3	155.2	145.0	133.7	124.1	116.5	130.3	143.7	144.0	162.7
2	1	180.9	169.1	146.2	124.1	115.3	120.1	137.5	148.6	159.7	161.5
3	1	190.0	154.6	135.8	118.8	115.2	124.9	140.2	132.4	150.7	168.8
4	2	171.5	149.9	133.6	124.3	123.2	129.2	149.2	141.0	141.7	162.3
5	2	170.5	154.8	137.6	124.6	122.3	121.8	144.9	143.9	160.2	150.5
6	2	172.6	146.7	136.9	128.2	129.6	140.9	150.4	145.5	161.6	169.5
7	3	184.9	165.7	141.0	138.6	126.5	140.7	146.3	148.9	163.2	160.0
8	3	183.7	158.3	136.0	130.8	126.6	132.1	157.3	144.3	152.4	165.8
9	3	188.9	168.2	155.4	145.6	134.1	128.8	135.7	177.9	187.2	160.8
10	4	176.5	155.8	137.0	121.9	114.1	108.1	113.6	132.6	129.4	153.4
11	4	176.5	153.1	141.7	136.0	126.2	117.0	125.1	131.9	141.4	162.2
12	4	179.6	163.8	151.6	135.2	127.0	117.7	139.0	135.7	155.5	153.4
13	5	177.6	146.9	131.6	119.8	122.0	119.9	130.5	149.0	143.3	164.8
14	5	183.6	133.6	126.0	125.8	122.4	128.2	129.1	148.7	148.9	150.3
15	5	187.8	164.9	133.0	127.5	124.3	111.9	117.2	140.9	132.6	157.2
16	6	173.8	156.6	130.4	119.9	118.7	111.7	111.2	135.6	142.7	164.6
17	6	179.1	154.2	126.0	118.1	116.1	117.8	121.7	141.5	145.1	163.1
18	6	178.4	153.0	129.7	125.0	116.9	119.4	120.4	138.1	153.2	165.0

Continued.....

TABLE II (Continued)

Shell Number	Bird	Shell level 0.02	0.10	0.20	0.30	0.40	0.50	0.60	0.70	0.80	0.90
19	7	165.6	139.3	124.4	126.5	129.0	129.7	137.8	152.3	153.5	143.6
20	7	177.2	154.4	143.0	121.0	126.0	118.8	128.3	135.7	129.3	161.0
21	7	166.9	155.6	132.4	130.1	124.6	123.6	128.5	139.0	142.6	155.3
22	8	172.4	153.3	139.6	124.7	124.1	123.9	135.4	150.2	148.6	161.2
23	8	185.7	148.5	136.1	124.0	120.6	121.2	127.8	141.7	153.6	180.4
24	8	174.6	161.2	134.2	122.5	118.7	121.4	133.2	132.4	160.9	170.4
25	9	174.1	144.6	132.4	118.7	114.4	115.7	121.0	126.8	130.4	142.7
26	9	159.6	162.2	144.0	120.6	121.9	115.6	135.3	141.6	150.6	152.7
27	9	186.4	160.7	140.7	127.8	121.1	124.9	134.9	134.6	155.0	146.3

TABLE III. ANALYSIS OF VARIANCE IN HARDNESS DATA

Source of Variation	Degrees of Freedom	Mean Square	F-Ratio
Shells	(26)	275.9	5.07**
- Birds	8	627.1	11.52**
- Shells in birds	18	119.8	2.20**
Shell levels	9	8792.	161.55**
Error	234	54.4	
Total	269		

** Significant at $P < 0.01$

Hardness differs significantly ($P < 0.01$) in different egg shells as shown by analysis of variance (Table III). Significant differences ($P < 0.01$) were found among successive shells from the same bird and among shells produced by different birds.

The gradient of hardness across the thickness of the shell is particularly noteworthy. For the cubic function fitted to the pooled data, the minimum occurs at shell level 0.40 with a value of 122.5 kg/mm^2 while surface hardness, by extrapolation, is 184.6 and 166.9 kg/mm^2 for outer and inner surfaces which represent increases of 51 and 36 percent respectively. The direct relation between hardness and strength of crystalline materials is well known (T1) and the

importance of shell hardness to crushing strength of eggs has been reported (T3). Gradients of hardness similar to those in egg shells are common in case-hardened metals (see, for example, p. 175 in reference M3) which possess durable surfaces, while the core is soft so that the material maintains a high shock resistance. The gradient of hardness in egg shells may be of fundamental importance to the strength of the egg; however, direct evidence of this is not available at present.

Results of Chemical Composition by Solution Methods

Percentage composition as oxides of calcium, magnesium and phosphorus along with estimated organic content for each shell appear in Table IV. These results show relatively close agreement with egg shell composition reported elsewhere (R2, S8). It should be noted that small amounts of other elements may occur in the shell, although their presence was not determined.

Results of Electron Probe Microanalyses

Electron beam scans

Large amounts of calcium, uniformly distributed through the shell, are evident in the electron beam scan of figure 2. Figures 3 and 5 show that magnesium occurs in solid solution with the calcium carbonate and that slightly higher concentrations may be present in a zone near the outer edge of the shell. The phosphorus content (figure 4) is

TABLE IV PERCENTAGE COMPOSITION OF EGG SHELLS BY SOLUTION METHODS

Shell	CaO	MgO	P_2O_5	Organic Matter *
1	52.87	0.713	0.588	2.97
2	52.58	0.705	0.515	3.04
3	52.49	0.656	0.611	3.23
4	52.86	0.476	0.485	3.14
5	51.67	0.584	0.487	4.00
6	52.19	0.618	0.517	3.25
7	52.26	0.607	0.462	3.37
8	51.61	0.561	0.694	3.75
9	51.88	0.597	0.586	3.11
10	51.74	0.552	0.532	3.86
11	51.99	0.630	0.587	3.43
12	51.92	0.677	0.610	3.65
13	51.26	0.642	0.473	4.14
14	51.70	0.561	0.422	3.39
15	51.50	0.605	0.617	2.96
16	51.72	0.754	0.629	5.38
17	51.57	0.648	0.468	3.57
18	51.57	0.638	0.428	3.62
19	52.18	0.547	0.499	3.12
20	51.49	0.633	0.541	3.81
21	51.94	0.579	0.479	3.22
22	51.99	0.767	0.426	3.30
23	52.07	0.686	0.541	3.15
24	51.28	0.614	0.559	4.25
25	52.30	0.586	0.494	3.49
26	52.00	0.665	0.595	3.08
27	52.80	0.586	0.507	2.47
Average	51.98	0.625	0.532	3.47

* Organic matter estimated by difference.

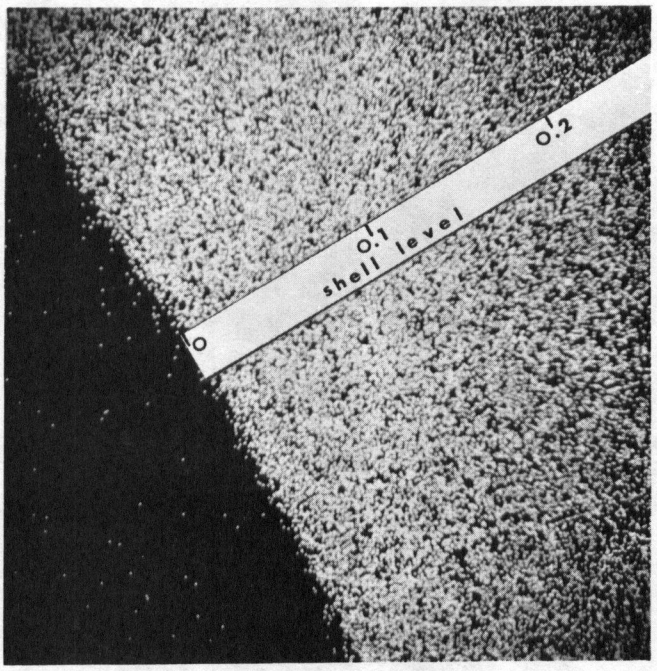

Figure 2. Calcium K_α electron beam scan at the outer edge of an egg shell. (790x)

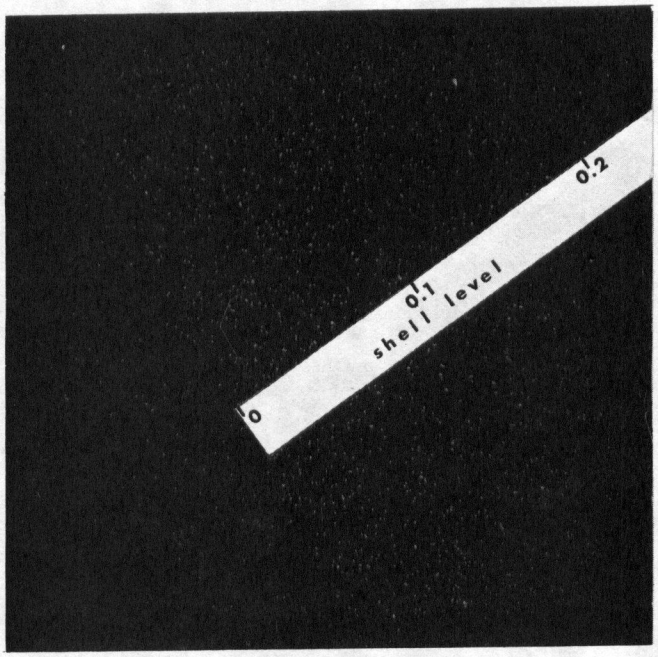

Figure 3. Magnesium K_α electron beam scan at the outer edge of an egg shell. (790X)

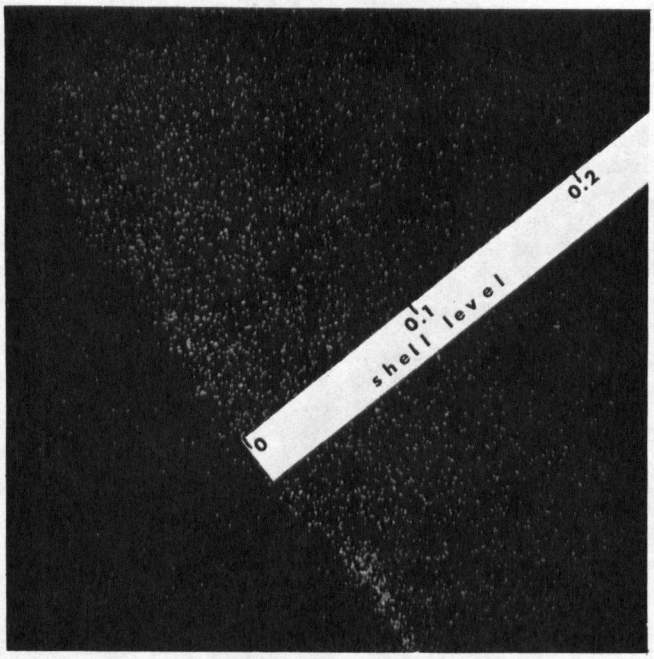

Figure 4. Phosphorus K_α electron beam scan at the outer edge of an egg shell. (790X)

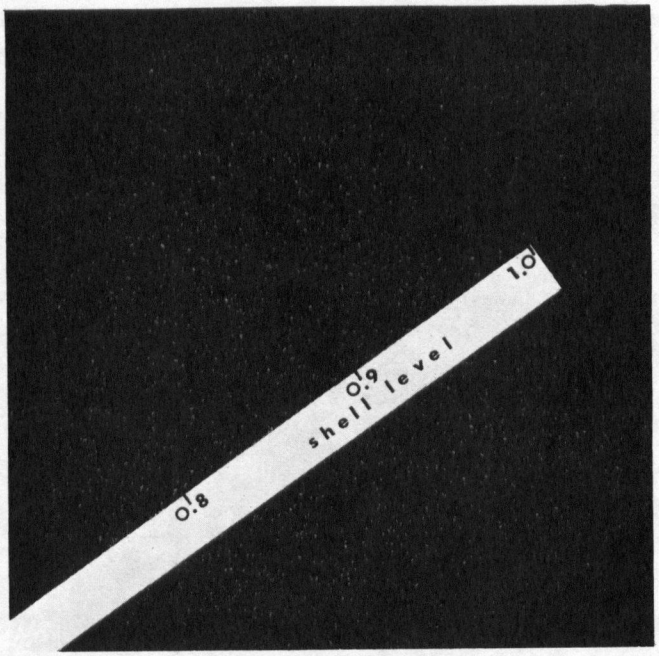

Figure 5. Magnesium K_α electron beam scan at the inner edge of an egg shell. (790X)

relatively high near the outer surface of the shell and decreases rapidly toward the shell interior. Several crystal boundaries are included in the electron beam scans but no differences are evident in calcium, magnesium or phosphorus content between crystals and their boundaries. Thus, step-scans on radial sections of the shell should be representative of composition across the egg shell thickness.

Step-scans across the shell

To test whether a single step-scan across the thickness of a shell adequately represents its composition, three separate step-scans were made in different positions along the equator of one shell. Analysis of the variance in composition at ten shell levels showed no significant difference ($P > 0.05$) among the mean MgO and P_2O_5 content of the three separate step-scans of one shell.

Mean values of percentage CaO, MgO and P_2O_5 at the ten analyzed shell levels were taken to represent the average composition of each shell (Table V). Egg shell composition varies considerably across the thickness of the shell as shown by average results at ten shell levels (Table VI). Tests of the composition-shell level relation show that calcium oxide content increases toward the inner surface of the shell (figure 6) as described by the equation

$$CaO = 51.24 + 3.13X \qquad [17]$$

where CaO = percent calcium oxide by weight.

For equation [17] the standard error of estimate is 1.27.

TABLE V. AVERAGE PERCENTAGE COMPOSITION OF EGG SHELLS BY ELECTRON PROBE MICROANALYSIS

Shell	CaO	MgO	P_2O_5	Organic Matter*
1	51.38	0.645	1.138	6.82
2	52.51	0.608	0.779	4.90
3	52.30	0.474	0.816	5.56
4	53.52	0.266	0.432	3.84
5	53.73	0.399	0.402	3.19
6	52.90	0.428	1.108	4.56
7	53.34	0.432	0.455	3.81
8	53.35	0.523	0.716	3.59
9	53.06	0.447	0.490	4.28
10	53.01	0.744	0.617	3.74
11	52.73	0.510	0.481	4.73
12	52.54	0.498	0.566	5.11
13	52.65	0.471	0.363	4.98
14	52.82	0.354	0.410	4.91
15	52.15	0.541	0.496	5.72
16	52.42	0.569	0.507	5.17
17	53.20	0.465	0.400	4.00
18	53.02	0.472	0.345	4.31
19	52.07	0.318	0.507	6.32
20	52.97	0.302	0.428	4.75
21	52.43	0.389	0.499	5.53
22	52.35	0.579	0.410	5.28
23	52.56	0.449	0.496	5.16
24	51.77	0.355	0.869	6.75
25	50.42	0.425	0.634	9.04
26	52.89	0.590	0.611	4.28
27	53.61	0.322	0.305	3.57
Average	52.65	0.466	0.566	4.96

* Organic matter estimated by difference.

TABLE VI. AVERAGE PERCENTAGE COMPOSITION AT TEN SHELL LEVELS IN 27 EGG SHELLS BY ELECTRON PROBE MICROANALYSIS

Shell level	CaO	MgO	P_2O_5	Organic Matter*
0.02	50.57	1.166	2.657	7.06
0.10	52.68	0.938	0.888	3.90
0.20	52.11	0.702	0.462	5.45
0.30	52.02	0.537	0.363	5.96
0.40	51.89	0.401	0.308	6.48
0.50	52.33	0.315	0.271	5.87
0.60	53.37	0.205	0.249	4.25
0.70	53.67	0.077	0.180	3.99
0.80	54.06	0.062	0.134	3.33
0.90	53.85	0.255	0.147	3.30
Average	52.66	0.466	0.566	4.96

* Organic matter estimated by difference

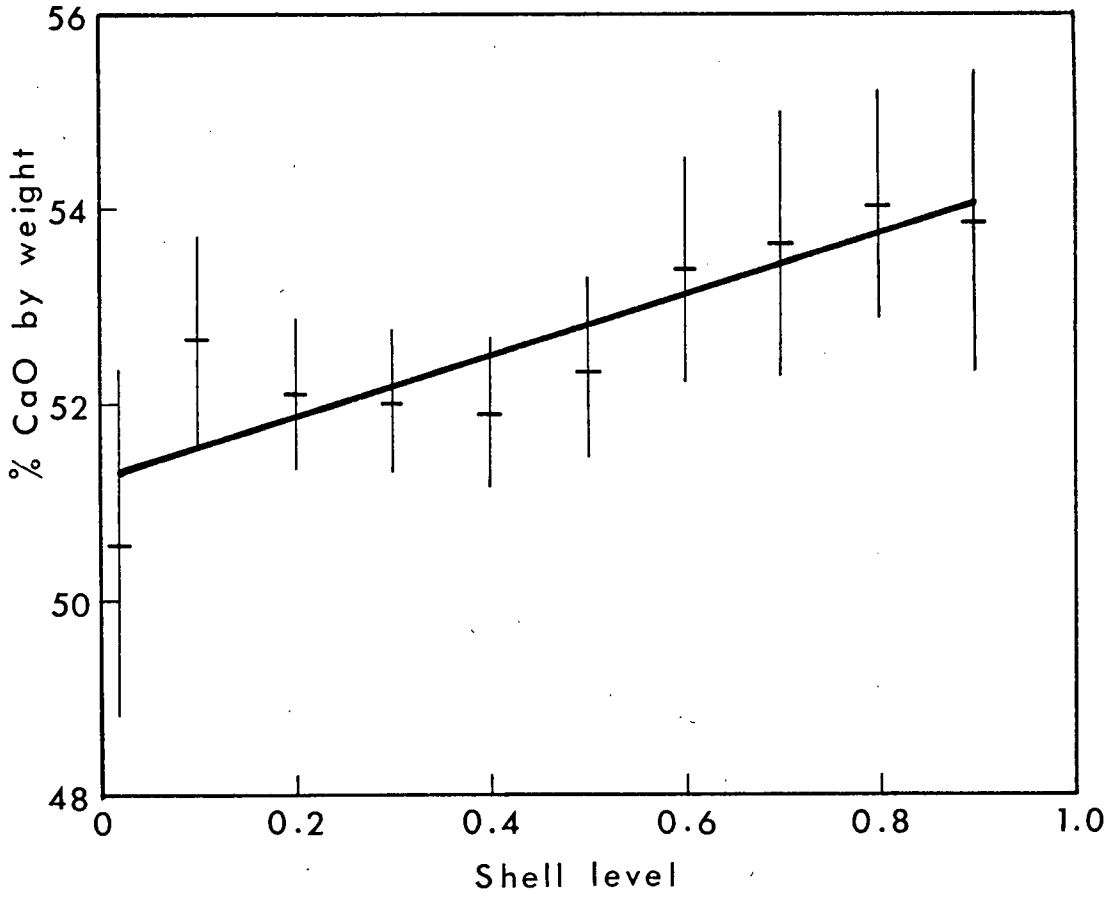

Figure 6. CaO content of 27 egg shells. The mean ± one standard deviation is shown at each shell level.

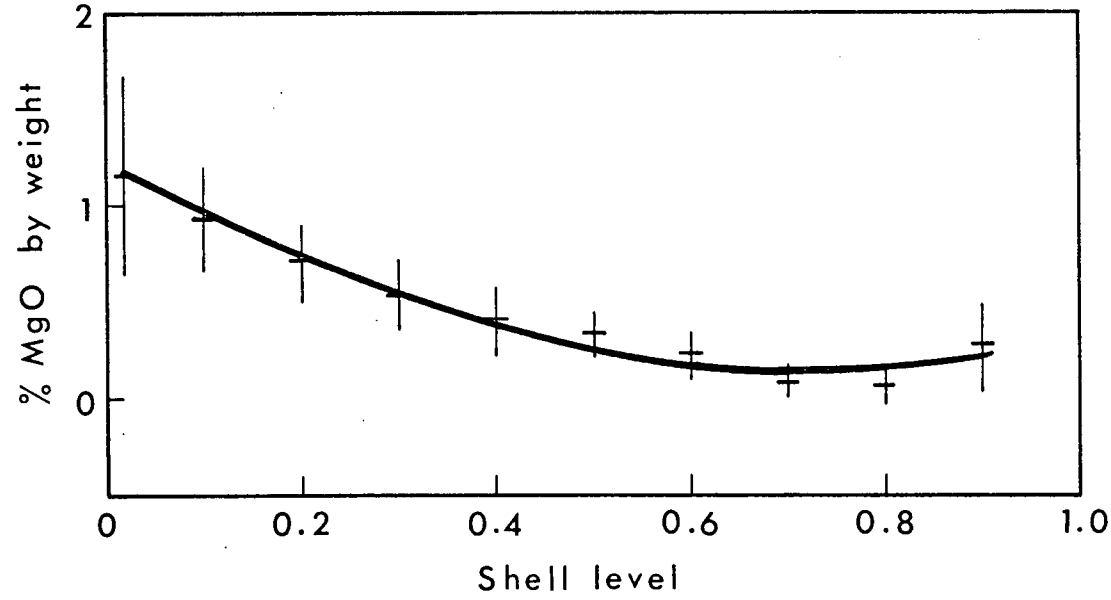

Figure 7. MgO content of 27 egg shells. The mean ± one standard deviation is shown at each shell level.

Magnesium oxide content is a maximum at the outer surface, falls to a minimum at shell level 0.75, then increases toward the inner shell surface. The gradient (figure 7, equation 18) is quadratic with a standard error of estimate of 0.23.

$$MgO = 1.22 - 2.86X + 1.89X^2 \qquad [18]$$

where MgO = percent magnesium oxide by weight.

Phosphorus concentrations are high near the outer surface of the egg shell and follow an exponential decrease (figure 8) given by

$$P_2O_5 = 0.143X^{-0.721} \qquad [19]$$

where P_2O_5 = percent phosphorus pentoxide by weight

X = shell level

Analysis of the variance (Table VII) in the composition data shows that calcium and magnesium contents are significantly different ($P < 0.01$) for the shells of different birds and for successive shells from a single hen; however, the phosphorus data do not show significant differences. Highly significant differences in chemical data among ten positions across the thickness of egg shells reflect the presence of calcium, magnesium and phosphorus composition gradients discussed earlier.

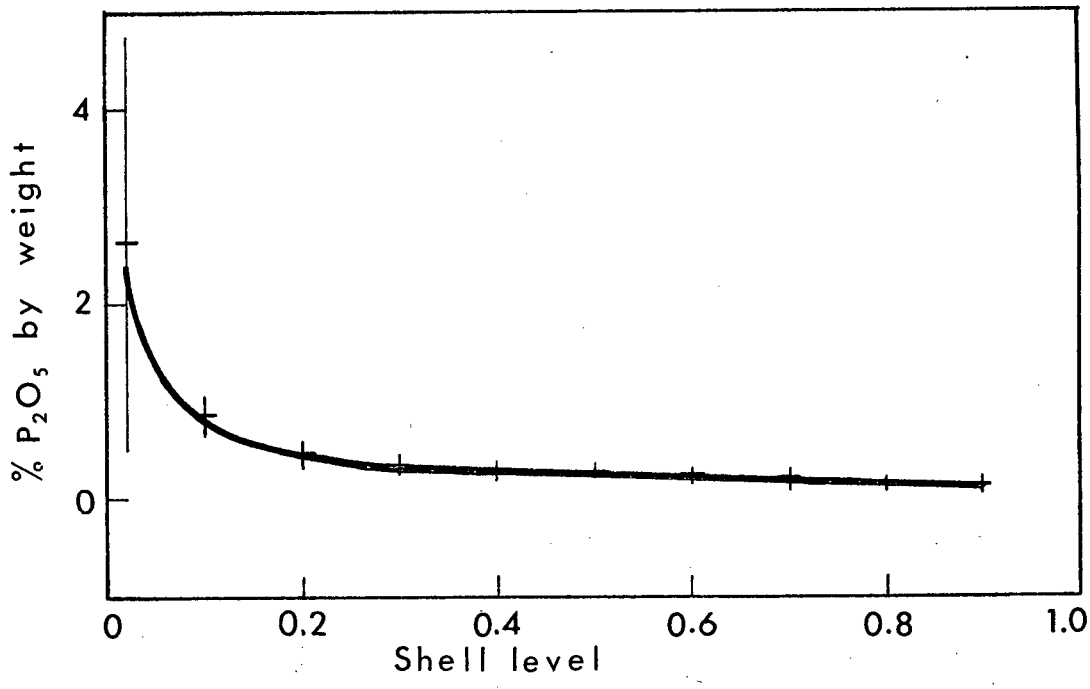

Figure 8. P_2O_5 content of 27 shells. The mean ± one standard deviation is shown at each shell level.

TABLE VII. F-RATIOS FROM ANALYSES OF THE VARIANCE IN COMPOSITION OF EGG SHELLS BY ELECTRON PROBE MICROANALYSIS

Source of Variation	Degrees of Freedom	CaO	MgO	P_2O_5
Shells	(26)	5.17**	2.98**	1.05ns
- Birds	8	6.32**	4.84**	1.53ns
- Shells in birds	18	4.67**	2.16**	0.83ns
Shell levels	9	32.73**	86.69**	36.13**
Error	234			
Total	269			

** Significant at $P < 0.01$

ns Not significant at $P < 0.05$

Comparison of Chemical Analyses by Solution Methods and the Electron Microprobe

The 27 sets of composition data, obtained by analyzing egg shell solutions (Table IV), were compared with corresponding electron probe results (Table V) using t-tests of their means. CaO and MgO determinations show significant differences ($P < 0.01$) for the two methods, whereas P_2O_5 compositions are essentially the same. Lower MgO values by the electron probe method are expected because the average is based on composition between shell levels 0.0 and 0.95 and magnesium content is known to increase at the inner shell surface (H7, T6). Furthermore, the solution methods included egg shell samples from the poles of the shell whereas electron probe analyses were restricted to the equator. Since the physical structure of the shell varies along its length [for example, thickness (T8) and porosity (W1)], the chemical nature may also change. The significant correlation coefficient of 0.525 ($P < 0.01$) between the pairs of MgO compositions indicates a linear relation between the two methods.

Relation of Hardness to Chemical Composition

Hardness proved to be a curvilinear function of calcium, magnesium and phosphorus content, thus multiple curvilinear regressions were used to determine the relation of hardness to composition in the pooled data for ten shell levels in 27 egg shells. Of the three chemical constituents in the regressions (Table VIII), magnesium contributes least to the explanation of variance in hardness, while variation in calcium is the most important contributor. When the data are considered on a pooled basis, the coefficient of multiple determination is 0.482; thus, there is an appreciable residual variance in hardness after chemical composition is considered.

Examination of the hardness-composition relation in the data of individual shells reveal different regressions from shell to shell. Coefficients of multiple determination (Table IX) indicate that, on the average, 90.9 percent of the variation in hardness can be explained by variations in calcium, magnesium and phosphorus in the same shell. When two of the chemical constituents are considered the average increase in explanation of residual variance by including the third component in the regression is 51.3, 49.5 and 63.0 percent for calcium, magnesium and phosphorus respectively; therefore, each of the three is important to the regression.

TABLE VIII. MULTIPLE CURVILINEAR REGRESSIONS OF HARDNESS ON COMPOSITION - POOLED BASIS (n = 270)

Independent Variable	Regression coefficient 1	2	3	4
CaO†	-133.14**	-190.6**	-134.5**	-
$(CaO)^2$	1.312**	1.848**	1.326**	-
MgO	- 3.448ns	8.704ns	-	- 19.98**
$(MgO)^2$	4.115ns	8.868**	-	10.75**
P_2O_5	25.91**	-	28.21**	25.30**
$(P_2O_5)^2$	- 2.614**	-	- 2.816**	- 2.597**
Constant	3500.	5046.	3532.	136.6
Sy††	13.96	15.33	13.96	15.94
R^2†††	0.482	0.371	0.478	0.320

** Significant at P < 0.01

ns Not significant at P < 0.05

† Percentage compositions by weight are used in the regression for the indicated compounds

†† Standard error of estimate

††† Coefficient of multiple determination

TABLE IX. COEFFICIENTS OF MULTIPLE DETERMINATION FOR REGRESSIONS OF HARDNESS ON COMPOSITION-INDIVIDUAL SHELL BASIS (n = 10)

Independent Variables	Range	Mean
Ca, Mg, P†	0.771 - 0.993	0.909
Ca, Mg	0.419 - 0.968	0.754
Ca, P	0.490 - 0.940	0.820
Mg, P	0.564 - 0.974	0.813

† Ca represents CaO and $(CaO)^2$, Mg represents MgO and $(MgO)^2$ and P represents P_2O_5 and $(P_2O_5)^2$ where percentage compositions by weight are used in the regressions for the indicated compounds.

Hardness is known to be a cubic function of shell level as given in equation [16] for which the coefficient of multiple determination is 0.795 on the pooled-data basis. Since chemical composition also varies across the thickness of the shell, regressions of hardness on composition and shell level were considered (Table X). The coefficient of multiple determination of 0.814 represents a 9.3 percent increase in explanation of residual variance due to inclusion of composition data. Another equally valid interpretation is that inclusion of shell level in the regression of hardness on composition explains an additional 64.1 percent of the residual variance in hardness. It is evident, therefore, that variations in hardness of egg shells are not entirely explained by variations in calcium, magnesium and phosphorus compositions across the thickness of egg shells.

Large improvements in regressions by including shell level suggest the presence of factors important to shell hardness that are associated with shell level. Two additional factors worthy of consideration are crystallite size and the organic matrix that extends through the egg shell. Crystallite size is reported to be much smaller toward the inner surface of the shell than near the outer surface (S2) and, for metals, hardness increases as the grain size decreases (H2). Organic matter is known to be

TABLE X. MULTIPLE CURVILINEAR REGRESSIONS OF HARDNESS ON COMPOSITION AND SHELL LEVEL - POOLED BASIS (n = 270).

Independent variable	Regression coefficient 1	2	3	4
CaO†	- 27.21ns	- 28.41ns	- 26.65ns	
$(CaO)^2$	0.279ns	0.290ns	0.273ns	
MgO	- 1.410ns	- 1.429ns		- 1.507ns
$(MgO)^2$	1.500ns	1.785ns		1.559ns
P_2O_5	1.617ns		2.620ns	- 0.181ns
$(P_2O_5)^2$	- 0.167ns		- 0.261ns	- 0.029ns
X††	-324.3**	-333.4**	-324.4**	-347.0**
X^2	529.3**	546.2**	531.3**	584.3**
X^3	-224.4**	-234.3**	-225.9**	-254.7**
Constant	842.7	877.1	827.1	184.6
Sy†††	8.42	8.39	8.40	8.78
R^2††††	0.814	0.814	0.814	0.796

† Percentage compositions by weight are used in the regression for the indicated compounds

†† Shell level

††† Standard error of estimate

†††† Coefficient of multiple correlation

ns Not significant at $P < 0.05$

** Significant at $P < 0.01$

present throughout the egg shell (S4) in the form of fibrils and vesicles, and there is evidence of histochemical differences across the thickness of the shell (S2). Mean values of estimated organic content obtained in this research (Table VI) show variations with shell level. These observations are suggestive; however, there is no direct evidence linking crystallite size and the nature of the organic matrix with hardness in the hen's egg shell.

SUMMARY AND CONCLUSIONS

Hardness and chemical composition were measured at ten positions across the thickness of 27 egg shells. Hardness varies in a curvilinear manner with maximum values at the outer surface, intermediate values at the inner surface and minimum values midway between. Calcium content increases toward the inside of the egg shell whereas magnesium and phosphorus are a maximum at the outer surface and follow quadratic and exponential gradients respectively.

For the data of individual shells, variation in chemical composition explains an average of 90.9 percent of the variation in hardness; however the relationship between hardness and composition differs from shell to shell. From the analysis of pooled data for all shells, variations in composition account for 48.2 percent of the variation in hardness. Inclusion of shell level in the regression increases the coefficient of multiple determination to 81.4 percent;

thus, additional unknown factors associated with shell level, may have an appreciable influence on egg shell hardness.

CHAPTER II. STRUCTURE OF EGG SHELL MEMBRANES

Egg shell membranes form a flexible leathery partition between the egg albumen and the shell. This structure consists of matted fibers with a combined thickness of about 65 microns (R3). Two layers are evident at the air cell region of the egg where the fibers separate to form the inner and outer membranes. At other locations in the egg, the membranes appear as a single layer; however, they may easily be pulled apart.

Although the inner membrane is thinner than the outer membrane (R3), the inner layer is more effective in preventing bacterial invasion of the egg (G1, L1). The object of this investigation was to elucidate the structure of the egg shell membranes with particular emphasis on differences between the inner and outer layers.

REVIEW OF THE LITERATURE

The fibrous nature of egg shell membranes has been known for over a century according to descriptions of early studies by light microscopy (N1, S8). Fiber diameters of 0.5 to 1.5 microns were reported; however, descriptions of fine structure were not possible at that time due to limitations imposed by the available microscopes.

Recent studies (M1, S4) of egg shell membranes by electron microscopy revealed two distinct regions in the cross section of individual fibers - an inner electron dense core and a lighter granular mantle surrounding the core. The core consists of α-keratin fibrils 30 to 40 Å in diameter and the mantle is thought to be a mucopolysaccharide material. The two regions are separated by an optically empty gap; however, it is not known whether the gap is present in the normal tissue or is an artifact resulting from the preparations for electron microscopy.

Observations on a transverse section through the membranes (S4) indicate that fiber diameters are somewhat larger in the outer membrane than in the inner. In a single plane section through the membrane, fibers are cut in cross section and longitudinally; thus, the fibers must run in varying directions throughout the membrane. At the inner surface of the inside membrane there is a thin layer of material that appears to be continuous over the surface. Experiments with fresh eggs have shown that this layer is impermeable to egg albumen (B9, N1); therefore, it may serve to exclude egg albumen from the spaces between fibers in the membrane.

In general, studies on egg shell membranes have been qualitative in nature with little information on fiber sizes and orientations along with the variations in these

characteristics at different positions in the membrane. The present experiment was initiated to provide quantitative measurements of fiber size and orientation in egg shell membranes.

EXPERIMENTAL METHODS

Preparation of Specimens

Two fresh eggs were randomly selected from the production of Single-Comb White Leghorn pullets (WL1 and WL2) and another two from New Hampshire pullets (NH1 and NH2). The eggs were opened, contents were discarded and albumen was washed from the egg interior using phosphate buffer solution (pH = 7.4).

Membrane samples were taken from the air cell region of each egg in such a manner that observations could be made on transverse sections that would be approximately latitudinal with respect to the egg geometry, that is, almost parallel to the egg equator.

A piece of the inner membrane was excised and placed in 3% gluteraldehyde-phosphate buffer solution for a 30 minute primary fixation. A small part of the shell with the adhering outer membrane was treated with the fixative for 90 minutes. Following fixation, membrane samples were washed in phosphate buffer. The egg shell was decalcified using a 6% solution of the disodium salt of ethylene diamine tetra-acetic (EDTA) containing 6% paraformaldehyde with the pH adjusted to 7.4

by sodium hydroxide. Membrane samples were then cut into small pieces and further fixed and stained for 2 hours with 1% osmium tetroxide in phosphate buffer. The tissue was dehydrated with a series of increasingly concentrated ethanol solutions, followed by replacement with propylene oxide, then infiltrated and embedded in Epon 812 (L3).

Transverse sections of the membranes were cut at 900-1500 Å with a Porter Blum ultramicrotome. The sections were picked up on carbon coated grids and stained for 15 minutes with uranyl acetate saturated in 70 percent methanol, then washed and stained for 10 minutes in lead citrate solution (R2).

Examination by Electron Microscopy

The sections were examined in a Philips 75C electron microscope at 60kV and images were recorded using an electron optical magnification of 830 diameters. Micrographs were printed at total magnifications of 6000 to 7000 times. Some higher magnifications up to 40,000 times were used to examine fine structure of the membranes. Transverse sections of the outer membranes were recorded by choosing several adjacent fields and preparing composites of the resulting micrographs. These methods provided views of complete transverse sections through both the inner and outer shell membranes of the four eggs.

Measurement of Membrane Dimensions

A coordinate system was applied to each transverse section by marking a rectangular area on the micrographs such that one pair of opposite sides coincided with the outer and inner boundaries of the membrane. Fiber dimensions (figure 9) were measured from micrographs of transverse sections for each of the four outer and inner membranes.

Many fibers were cut obliquely and appeared to be elliptical in the section. The mantle surrounding the fiber core was not of uniform thickness even in fibers cut at right angles to their major axes; thus, the least diameter of the elliptical section was assumed to be the true fiber diameter and fiber core dimensions were measured in preference to the combined core and mantle dimensions. Average mantle thickness was evaluated in the direction of the least diameter of the fiber section. Each fiber in the membrane section provided five measurements: fiber core diameter (d_c), maximum core diameter (d_m), average mantle thickness (t_m), the distance from the fiber center to the outside edge of the membrane section (x) and the angle between the outside edge of the membrane section and the major axis of the fiber cross section (ϕ).

Analysis of Data

Linear measurements from the micrographs were converted to actual dimensions in the tissue using the appropriate magnification factors. The position of the fiber

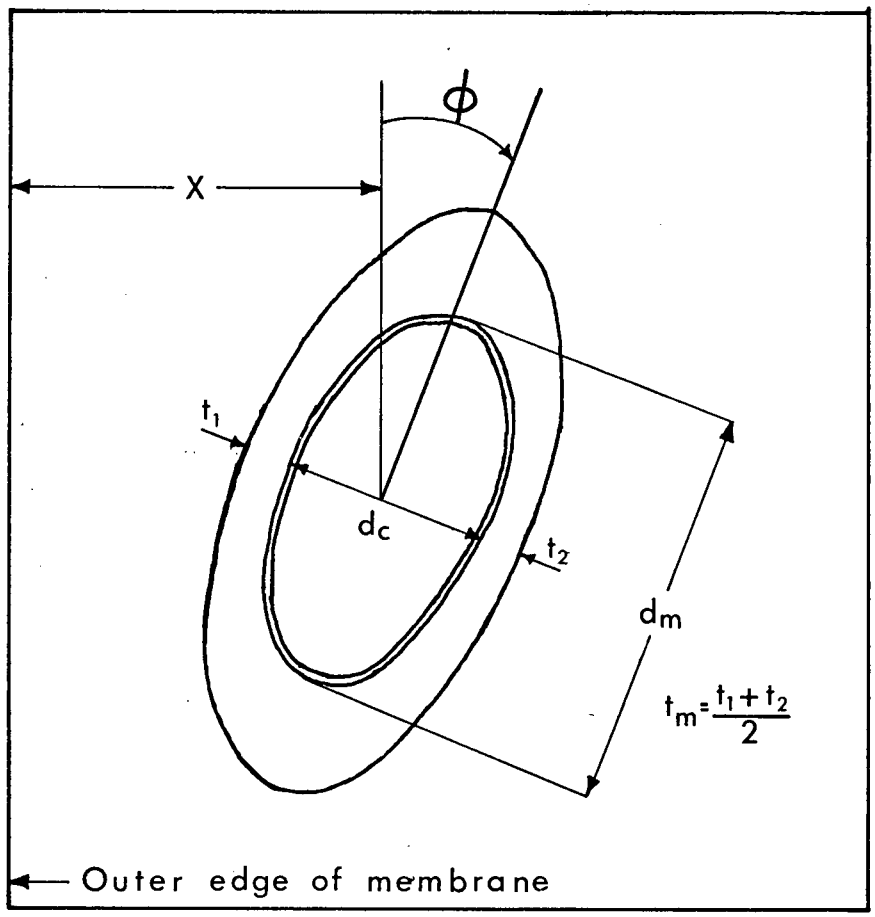

Figure 9. Schematic diagram of an oblique section through an egg shell membrane fiber to illustrate the dimensions measured.

in relation to the membrane surfaces was derived from the distance between the fiber center and the outside edge of the membrane. This dimension was divided by the total membrane thickness to give a number between 0 and 1.0 which was called membrane level.

The proportion of the transverse section occupied by fibers was computed for each membrane. Fibers were assumed to be circular in cross section with the mantle uniformly distributed around the fiber core. Thus, for fibers that passed through the plane of the section in a direction other than normal to the section, the exposed oblique sections were elliptical and the areas calculated accordingly. The ratio of total exposed fiber area and membrane section area was termed fiber area density.

Mean values of fiber core diameter and mantle thickness were computed for the outer and inner membranes of each egg. T-tests were used to determine whether the mean fiber core diameter and mantle thickness differ between outer and inner membranes of the same egg. Similar comparisons were also made among outer membrane dimensions and among inner membrane dimensions of the four eggs by means of t-tests.

The data for each membrane were then separated into portions according to membrane level in order to examine fiber dimensions at different locations across the thickness of the structures. On the basis of equal membrane

level intervals, data were divided into ten and four groups for outer and inner membranes respectively. Means and standard deviations were then computed for each group of data.

RESULTS AND DISCUSSION

Qualitative Observations on Membrane Structure

Earlier descriptions of egg shell membrane structure (M1, S4) are confirmed by this study. Individual fibers possess a central core surrounded by a mantle with a distinct separation between the two regions (figures 10 to 13). Higher magnifications reveal the orderly fibrous nature of the core in contrast to the granular appearance of the mantle. Mantle thickness is variable even for fibers cut in cross section. The mantle layer is often continuous around adjacent fibers and appears to cement fibers together where they cross. In a single section, fibers are cut in cross section and longitudinally as well as at angles intermediate to the two extremes; thus, the fibers travel in many directions to form a matted network.

At similar magnifications, fibers in the outer membrane appear larger than those of the inner membrane. For some pairs of membranes, particularly from the White Leghorn birds, there appears to be larger interfiber spaces in the inner membrane. Inside boundaries of inner membranes have a 0.1 micron thick layer of material similar in electron

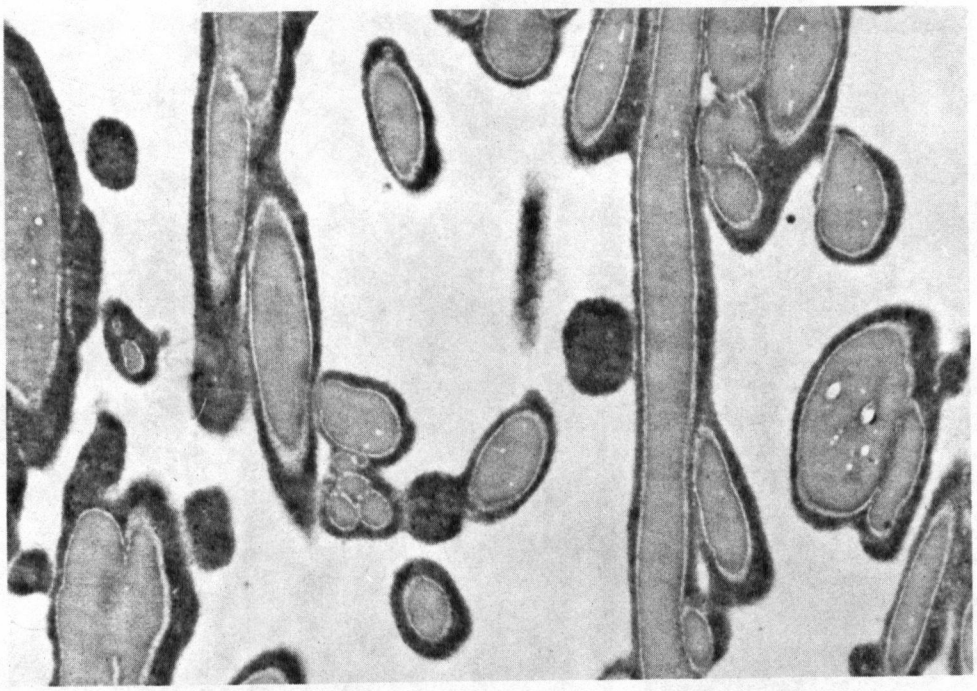

Figure 10. WL1 outer egg shell membrane (6660X).

Figure 11. WL2 inner egg shell membrane (6660X).

Figure 12. NH1 outer egg shell membrane (7050X).

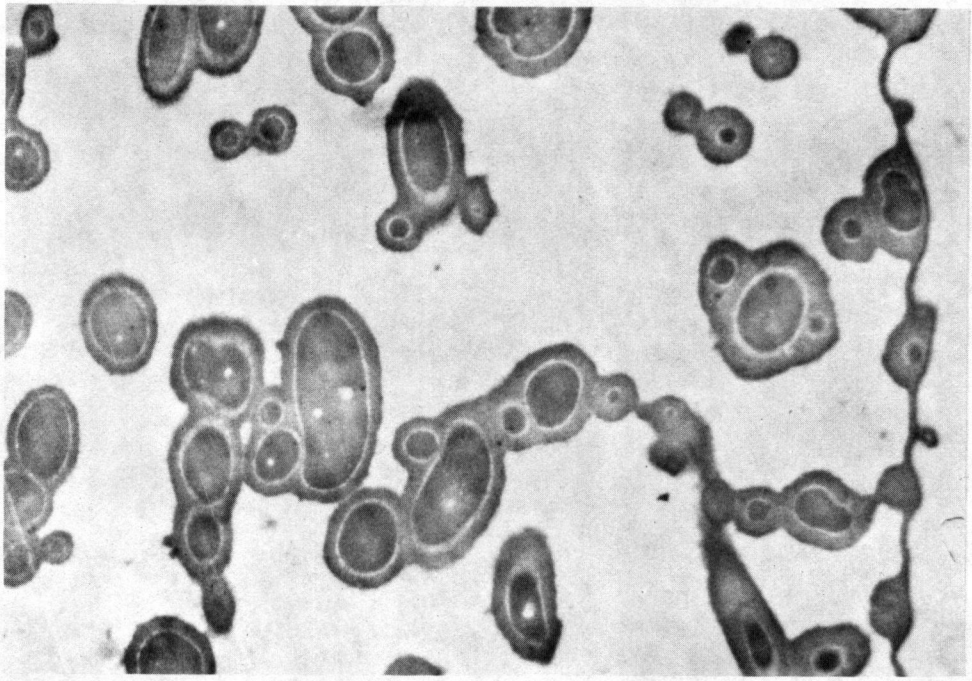

Figure 13. NH1 inner egg shell membrane (11200X).

density to the mantle substance (figures 11 and 13). The WL2 inner membrane has two layers separated by a narrow gap. Since the other membrane surfaces are of open structure and interfiber spacings are larger than bacterial dimensions, this continuous layer is the only visible physical barrier to microbial penetration of egg shell membranes.

Results of Measurements of Membrane Structure

Membrane thickness and fiber area density

Outer egg shell membranes are approximately three times as thick as inner membranes (Table XI). The combined structures range from 73 to 114 μ in thickness.

Fiber area density provides a measure of combined fiber size and spacing characteristics in the plane of the membrane section. For the membranes of the White Leghorn eggs, outer membranes have a fiber area density twice that of inner membranes. This result confirms the more open appearance of the inner membrane (figure 11) relative to the outer (figure 10). The closeness of the fiber area densities for the two NH1 membranes is reflected by their qualitative similarities evident in figures 12 and 13.

TABLE XI. THICKNESS AND FIBER AREA DENSITY OF EGG SHELL MEMBRANES

Membrane		Thickness, μ	Fiber area density†
WL1	- outer	53.2	0.554
	- inner	19.5	0.272
WL2	- outer	65.5	0.490
	- inner	24.3	0.238
NH1	- outer	91.8	0.369
	- inner	22.4	0.388
NH2	- outer	80.9	0.456
	- inner	27.7	0.331

† Fiber area density is defined as the ratio of total exposed fiber area and membrane section area.

Mean values of fiber measurements

The mean fiber core diameter (Table XII) of the outer membrane is significantly greater ($P < 0.01$) than the mean fiber core diameter of the inner membrane for each of the four eggs. Comparisons among corresponding WL1 and WL2 membranes indicate that mean fiber core diameters differ ($P < 0.01$) between the outer membranes whereas the inner membrane fiber core diameters are essentially the same ($P > 0.05$). T-tests of the NH1 and NH2 membranes reveal no significant differences ($P > 0.05$) of the mean fiber core diameters in the pair of outer membranes and in the pair of inner membranes. In all comparisons between corresponding membranes of the White Leghorn and New Hampshire eggs, mean fiber core diameters were significantly greater ($P < 0.01$) for the New Hampshire eggs.

The mean fiber mantle thickness in the White Leghorn eggs does not differ ($P > 0.05$) between outer and inner membranes nor between membranes of different eggs. Mantle thickness is greater in the inner NH1 membrane than in the outer membrane whereas the reverse is true for the NH2 membranes. In general, fibers in the New Hampshire membranes possess thicker mantles ($P < 0.01$) than those in White Leghorn membranes. The average coefficient of variation of 57.8 percent indicates that mantle thickness is highly variable in egg shell membranes.

TABLE XII. MEAN VALUES OF EGG SHELL MEMBRANE MEASUREMENTS

Membrane	Number of fibers measured	d_c†, microns	t_m††, microns	ϕ†††, degrees
WL1 - outer	459	0.681	0.105	-0.34
- inner	145	0.481	0.102	2.04
WL2 - outer	571	0.789	0.102	-0.76
- inner	222	0.475	0.096	-2.07
NH1 - outer	443	0.871	0.149	-3.22
- inner	152	0.574	0.172	0.53
NH2 - outer	433	0.842	0.151	1.57
- inner	128	0.592	0.120	1.37

† Diameter of fiber core

†† Thickness of fiber mantle

††† Angle between outer edge of membrane section and major axis of fiber cross section

It should be noted that fiber size is reported as fiber core diameter and average mantle thickness for reasons discussed earlier. Overall fiber diameter may readily be computed as the sum of fiber core diameter and twice the mantle thickness.

The angle ϕ (Table XII), between the outer edge of the membrane section and the major axis of an exposed section through a fiber, reflects the fiber direction in relation to the surfaces of the membrane. If fibers are assumed to be cylindrical, $\phi = 0°$ represents a fiber in a surface parallel to the membrane surfaces, whereas $\phi = \pm 90°$ describes a fiber passing diagonally across the thickness of the membrane. Since the mean value of ϕ for the fibers in each membrane approaches zero, fibers are located in surfaces approximately parallel to the membrane surfaces.

Variation in fiber measurements across the membrane

Average fiber core diameters at ten outer membrane levels and four inner membrane levels are shown in figures 14 to 17. No consistent trend is evident in mean fiber core diameter across the thickness of the four outer and the four inner membranes; however, fiber diameters are distinctly smaller for the inner membranes of each pair. For each of the intervals across the membrane, fiber core diameters show considerable variation as is illustrated in the figures by the vertical bars which represent the standard deviation.

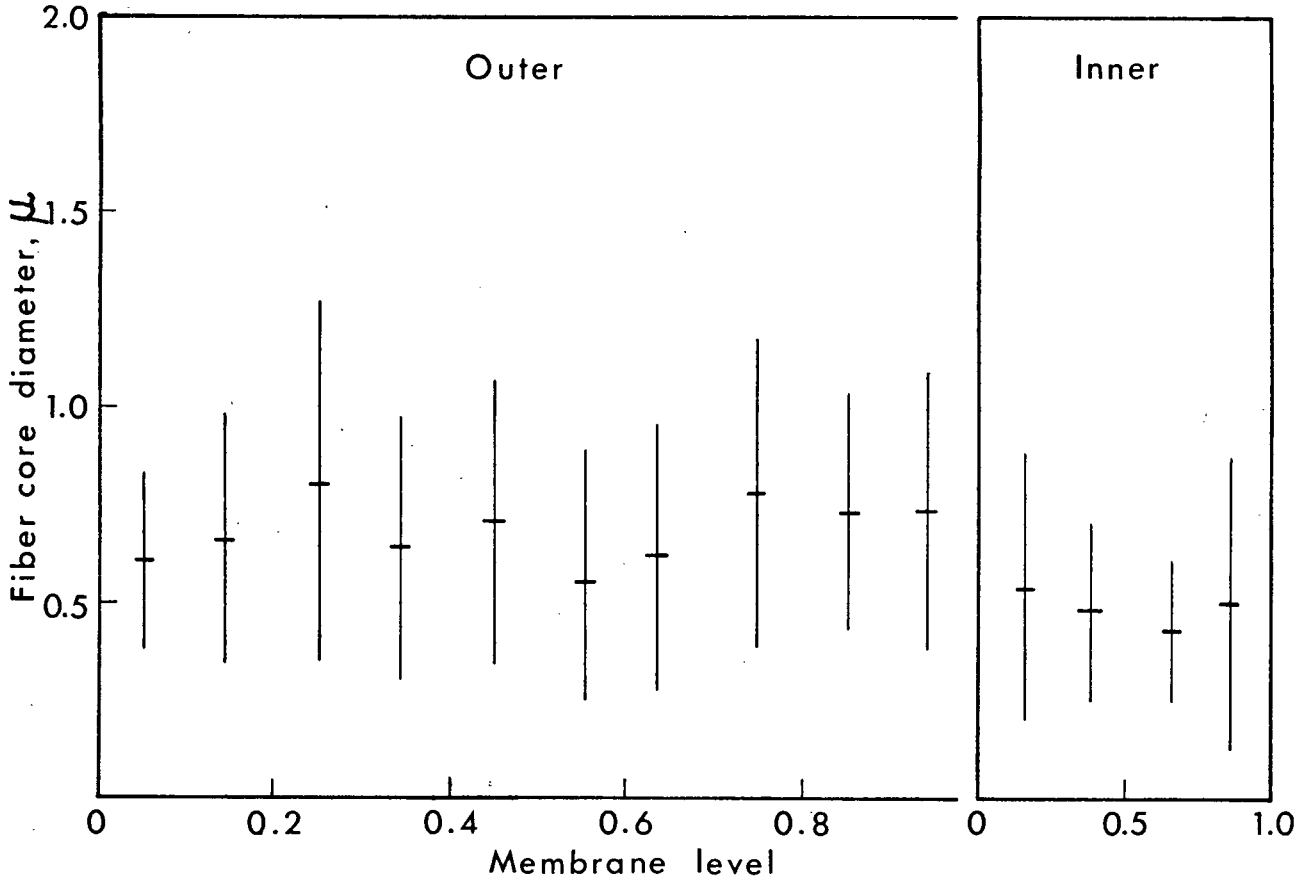

Figure 14. Fiber core diameters for membrane WL1. The mean and standard deviation at each level are shown.

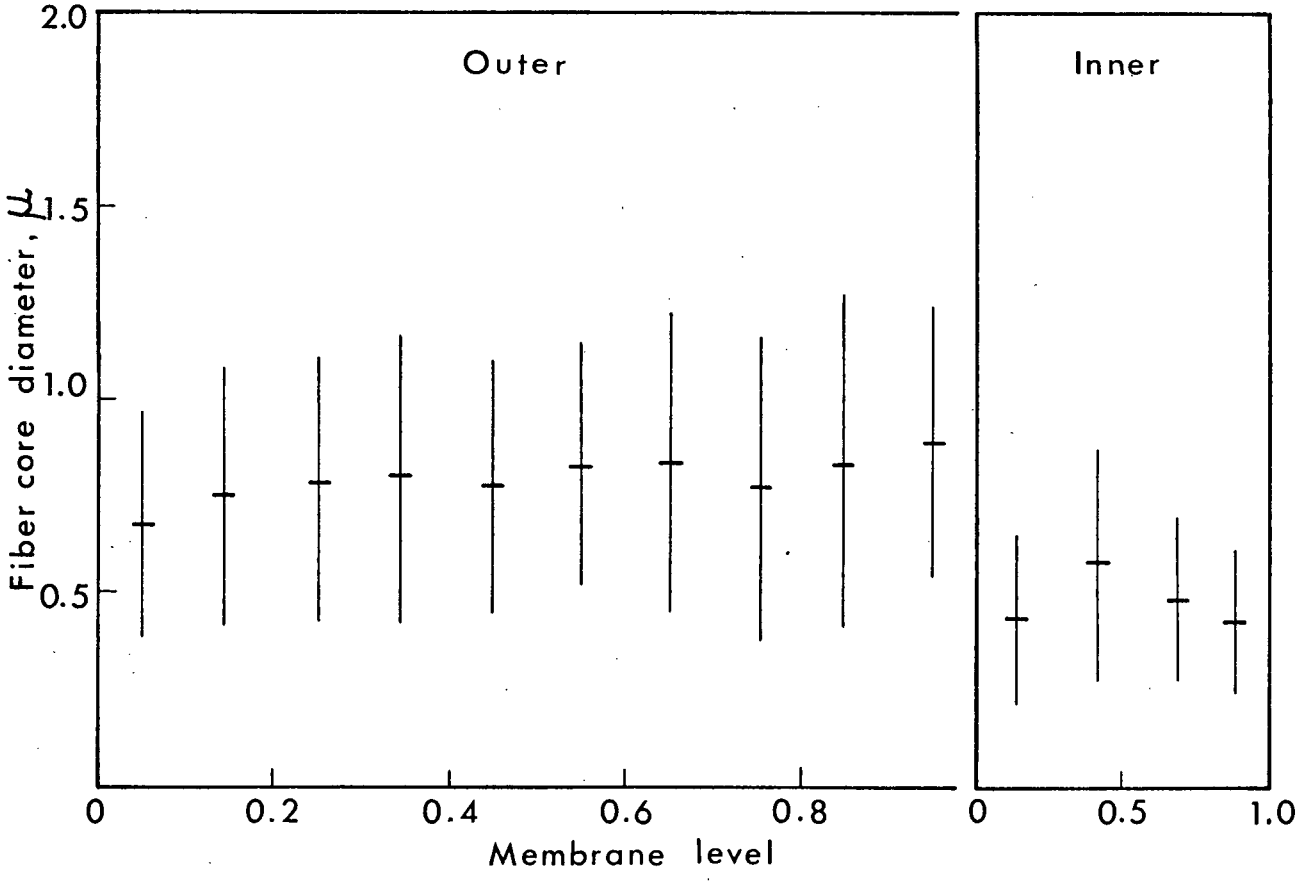

Figure 15. Fiber core diameters for membrane WL2. The mean and standard deviation at each level are shown.

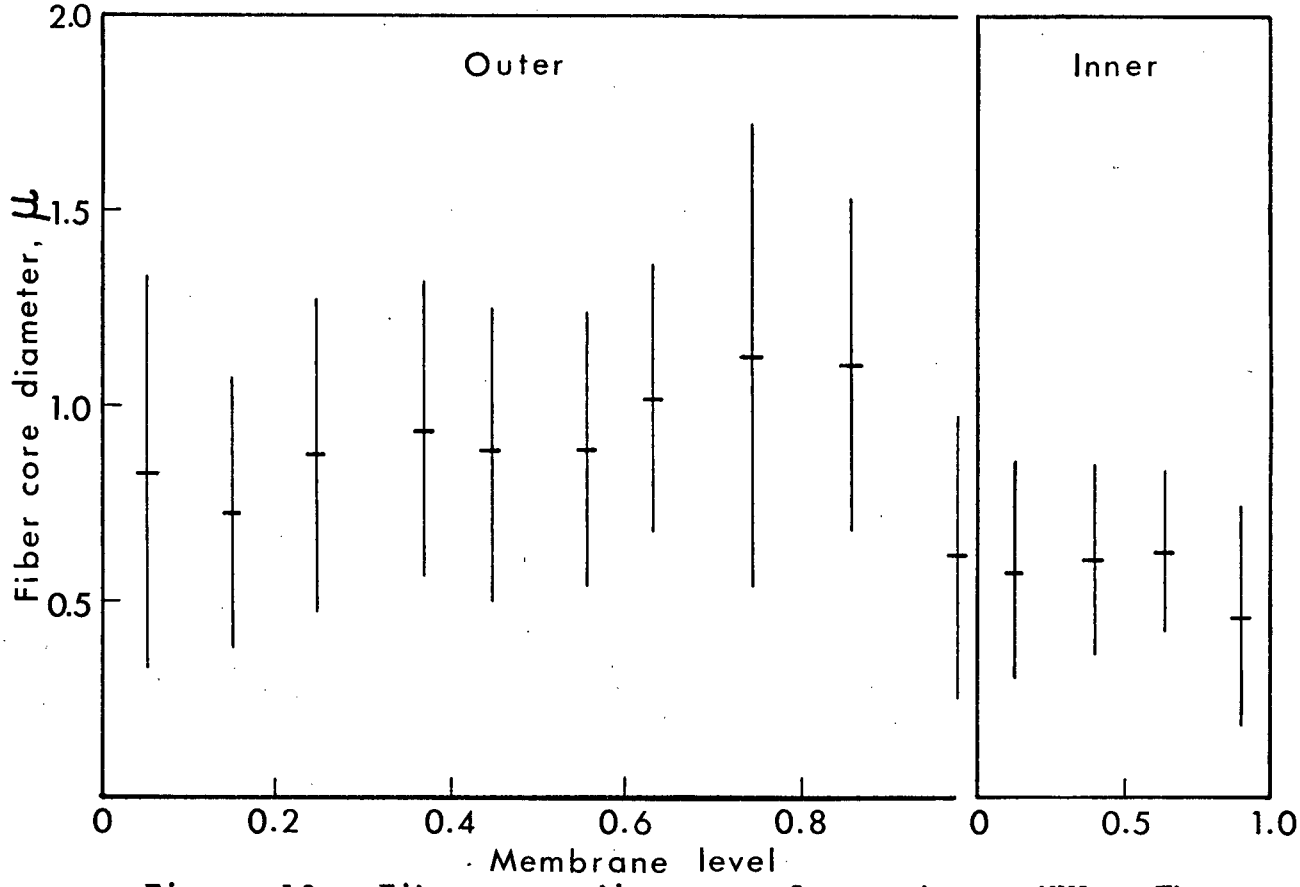

Figure 16. Fiber core diameters for membrane NH1. The mean and standard deviation at each level are shown.

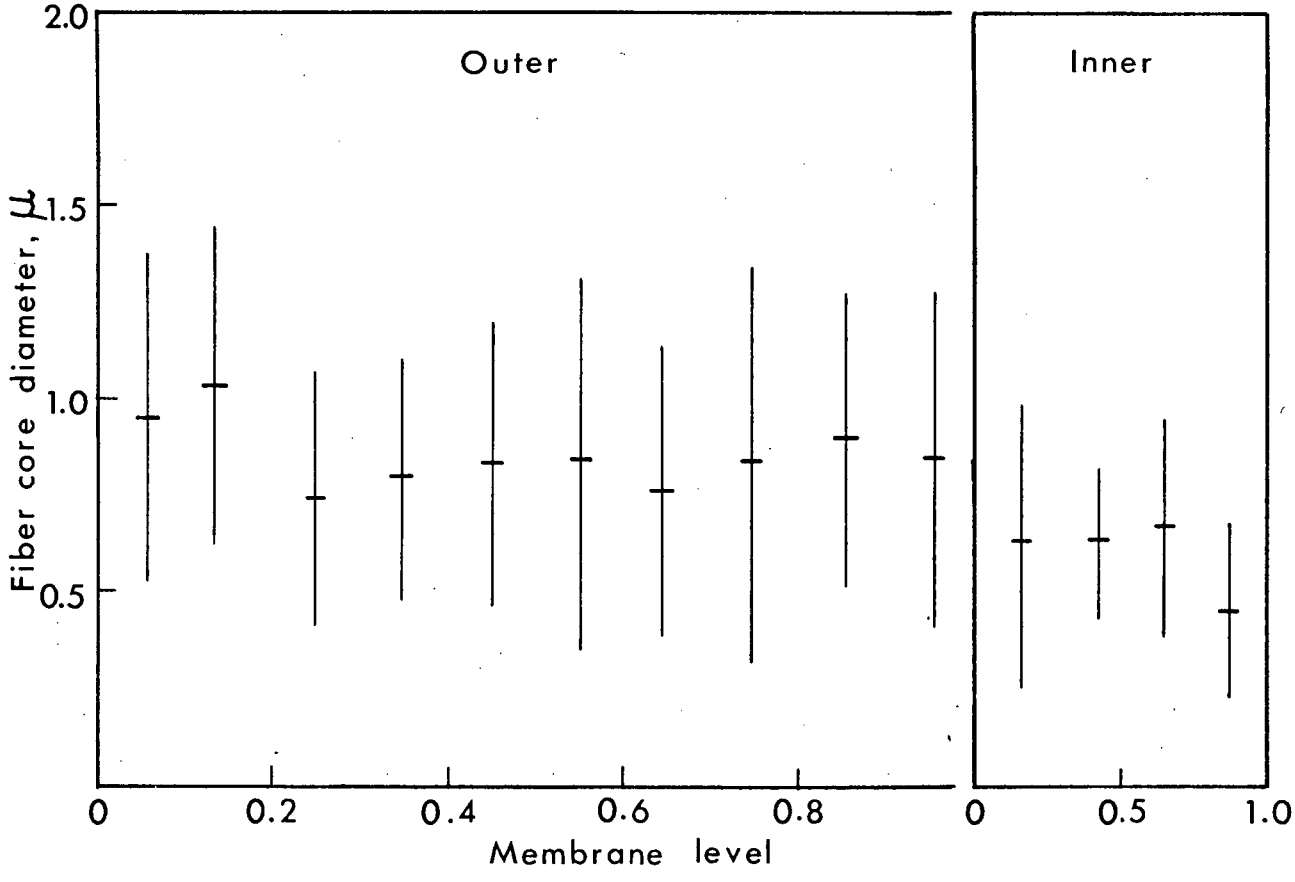

Figure 17. Fiber core diameters for membrane NH2. The mean and standard deviation at each level are shown.

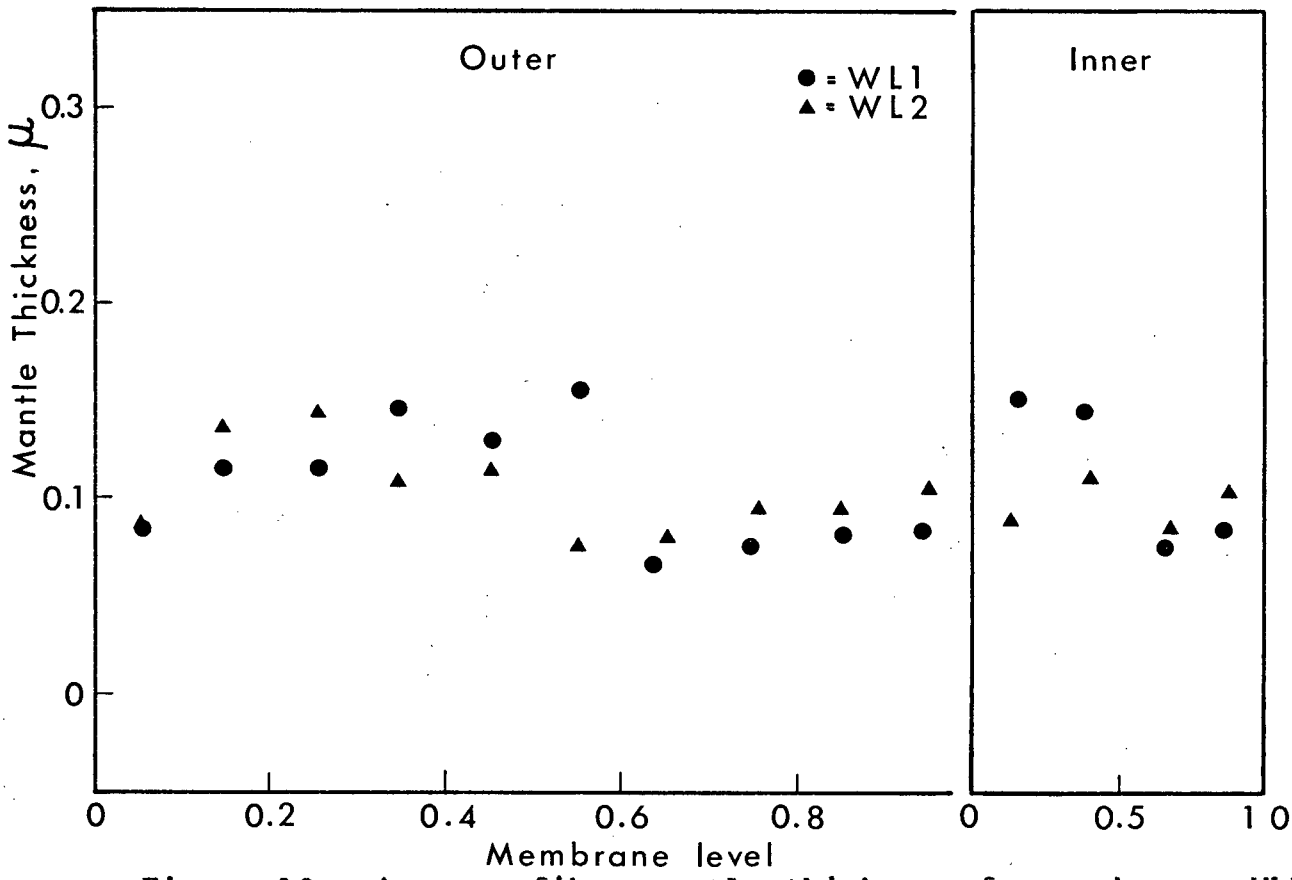

Figure 18. Average fiber mantle thickness for membranes WL1 and WL2.

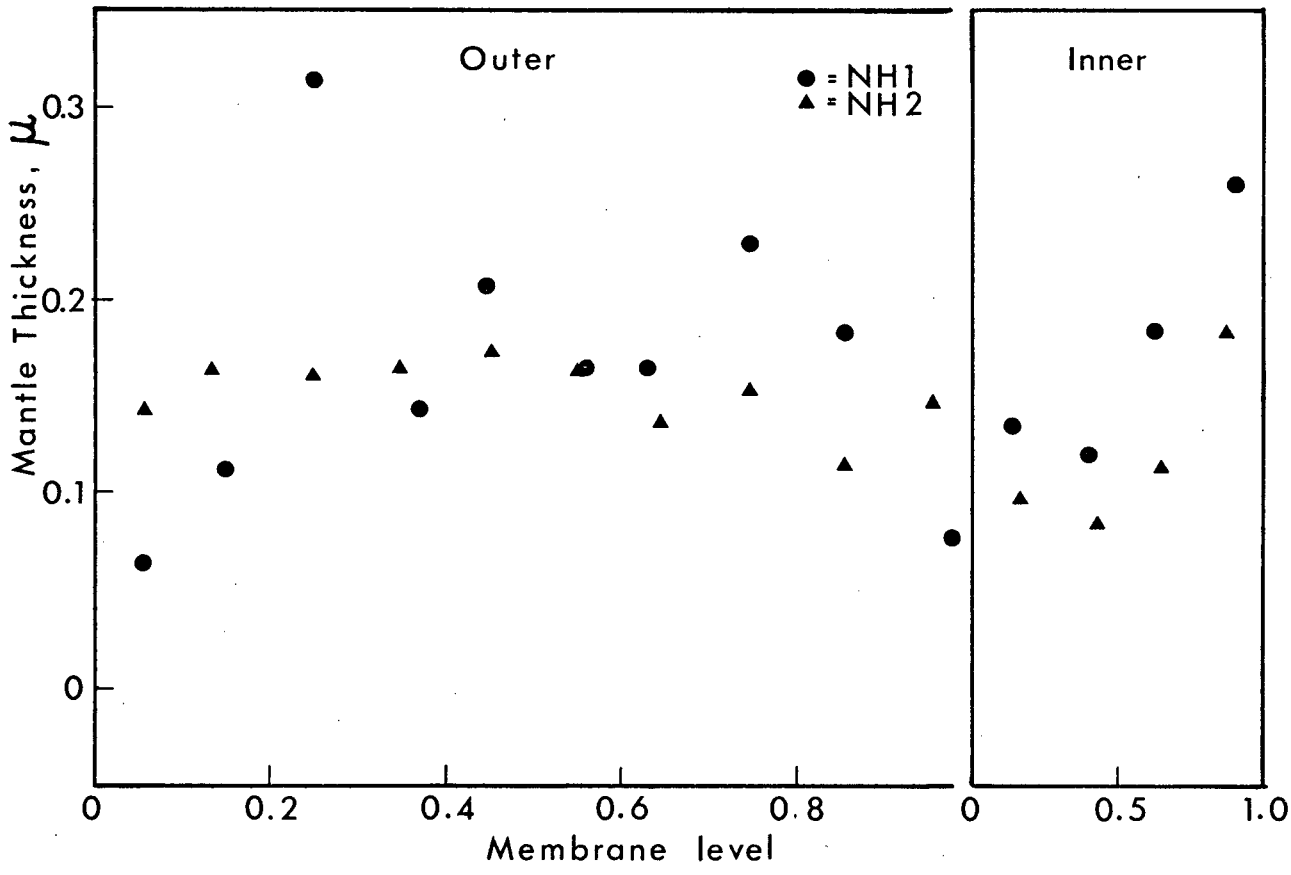

Figure 19. Average fiber mantle thickness for membranes NH1 and NH2.

The average mantle thickness fluctuates across the membrane (figures 18 and 19); however, the variations appear to be random.

SUMMARY AND CONCLUSIONS

The shell membranes of four eggs were subjected to electron microscopical examination at relatively low magnifications. Micrographs were assembled to permit measurements of position and dimensions for each fiber in transverse sections through the membranes.

Egg shell membranes consist of a fibrous network that is separated into two distinct layers. The outer membrane is three times as thick as the inner membrane and the combined structure is approximately 100 microns in thickness.

Fibers are oriented in many directions in surfaces that parallel the membrane surfaces. The fibers of outer membranes are larger than those of inner membranes and spacings among the fibers may differ from membrane to membrane.

A 0.1 micron continuous layer of tissue is present at the inside surface of the inner shell membrane. Since the remaining structures are an open network, this layer may be of fundamental importance in retarding bacterial penetration of egg shell membranes.

Individual fibers within the membranes possess a central core surrounded by a granular mantle of varying thickness. Fiber core diameters are significantly larger ($P < 0.01$) in the outer membrane than in the inner membrane of an egg.

Variations in fiber core diameter and mantle thickness occur across the thickness of egg shell membranes; however, these variations appear to be random.

CHAPTER III. RHEOLOGY OF EGG ALBUMEN

Rheological properties of fluid foods influence the design of materials handling and processing equipment. Since most foods have a complex viscous nature (C1, H4, L2, S1, W2) that changes with composition, temperature, shear rate and duration of shearing; studies of food rheology are largely empirical.

Three hundred million pounds of egg albumen are processed annually on this continent (F1) by means of operations that include separating, pumping, mixing, heating, cooling and spray drying; however, very little information is available on the physical properties of this fluid. Lack of adequate rheological characterization of egg albumen has undoubtedly been an obstacle in the design of processing equipment. The purpose of this research was to supplement available data on the viscous behavior of egg albumen.

REVIEW OF THE LITERATURE

Flow of egg albumen through capillary tubes under constant pressure has been used to compare consistencies of samples subjected to different experimental conditions (B1, S5). Such information is useful in detecting changes in viscosity; however, single point viscosity measurements do not characterize flow behavior over a range of shear rates as required for design purposes. Damping properties of intact eggs have been studied using a torsion pendulum

(A1, R4); however, the data show small correlations with the viscous nature of the egg components. The modulus of rigidity of thick albumen has been evaluated by means of the displacement of a small nickel sphere in a magnetic field and by torsion between concentric cylinders (B7).

Kaufman et al. (K1) cited unpublished data in which viscosity of commercial unfrozen egg products at pasteurization temperatures did not change greatly over a range of shear rates. Preliminary tests on thick and thin egg albumen, separately and combined, at temperatures up to 40°C, showed decreasing apparent viscosities with increasing shear rates. Shearing also causes a breakdown of structure during tests in a pressurized capillary viscometer (S5) and in a rotational viscometer at a constant rate of shear (T5). Thus egg albumen exhibits pseudoplastic, time-dependent flow behavior at moderate temperatures. The following experiments were designed to evaluate the rheological behavior of egg albumen over a moderate range of shear rates and temperatures.

EXPERIMENTAL METHODS

Preparation of Samples

Two lots of sixty fresh eggs were used in this experiment. Twenty randomly selected eggs from each lot were weighed, albumen height measured and Haugh score calculated (B5) to serve as a general indication of egg quality. The albumen from each lot of sixty eggs was combined and forced

six times through a number 3 Buchner funnel. This procedure homogenized the thick and thin portions of the albumen and was intended to simulate the commercial practice in which albumen is passed through a fine mesh screen to remove suspended materials. Samples were taken for measurements of pH and percentage solids (H6).

Test Procedures

Viscous properties were measured with a Haake rotational viscometer (V1) equipped with MVI and NV narrow-gapped concentric cylinder spindles and cups. The MVI spindle with a gap width of 0.96 mm provided a maximum shear rate of 1320 sec^{-1} whereas the NV spindle had a maximum shear rate of 3140 sec^{-1} and was double-gapped with widths of 0.70 and 0.80 mm. Calibration constants for the spindles were established by means of oil viscosity standards. Output from the dual-range torsion dynamometer was fed to a 10-inch, two channel, strip chart recorder through a switch that permitted selection of either recorder channel. One channel was calibrated at twice the sensitivity of the other to increase precision of measurement for smaller signals. Sample temperatures were maintained within $\pm$ 0.5°C by a thermostatically controlled water jacket surrounding the measuring head.

Each sample was first tested for time dependence by recording the shear-stress decay curve at a constant rate of shear. The shear-stress curve reached a maximum after one or two seconds due to recorder response and inertial effects, then appeared to follow a logarithmic decay to an

equilibrium value in five to ten minutes. When the shear stress reached a constant value, flow-behavior curves were obtained by decreasing the shear rate over a series of steps and then increasing the shear rate stepwise to the original value while recording the corresponding shear stresses. The maximum shear rate used in obtaining flow curves did not exceed the shear rate of the time-dependence tests.

The following tests were performed using one lot of egg albumen. Recovery of shear strength was investigated at 10°C in three samples sheared at a rate of 3140 sec^{-1}, after which the samples were stored in airtight plastic containers at 4°C for 32 hours and then retested under identical conditions. Shear rates of 1570 and 3140 sec^{-1} were used on triplicate samples to determine the influence of shear rate on the time-dependent characteristic.

The second lot of albumen was tested at temperatures of 10, 20, 30 and 40°C using each of the two spindles. Shear-stress decay curves and equilibrium flow-behavior curves were obtained for all tests and a total of three runs were made at each experimental condition.

Rheological Models

Models of time-dependent behavior

Data were sampled from the chart paper by a method (C2) designed to preserve data equally throughout its range. Since shear stress appeared to decrease logarithmically with time, the range between the initial usable maximum and the

equilibrium shear-stress was divided into ten equal logarithmic intervals and the corresponding stresses and times were recorded. For the purpose of analysis, η and $\eta-\eta_e$ were calculated for each datum, where η is apparent viscosity in poise and η_e is the apparent viscosity at equilibrium for a run. Data for the three runs at each experimental condition were pooled and treated as a single curve.

Using η and $\eta-\eta_e$ as dependent variables and time as the independent variable; linear, logarithmic and hyperbolic functions were tested for accuracy of fit to the data. Functions that suitably fitted the data were:

$$\eta = a_1 - b_1 \log t \qquad [20]$$

$$\log (\eta-\eta_e) = a_2 - b_2 t \qquad [21]$$

and

$$\log (\eta-\eta_e) = a_3 - b_3 \log t \qquad [22]$$

where t is time in seconds and a_1, a_2, a_3, b_1, b_2, b_3 are constants. Equations [20] and [21] are similar to models suggested by Weltmann (W4) and Hahn et al. (H1) for stress relaxation in thixotropic systems. Equation [22] was used in subsequent analyses because it described the data most accurately with an average coefficient of determination of 0.83 compared with 0.72 and 0.77 for Equations [20] and [21] respectively.

Models of flow-behavior

Equilibrium flow-behavior data were fitted by the well known power-law equation

$$\eta = m\dot{\gamma}^{n-1} \qquad [23]$$

or

$$\frac{1}{\eta} = \left[\frac{1}{m}\right]^{1/n} \tau^{(1/n)-1} \qquad [24]$$

where η = apparent viscosity, poise

$\dot{\gamma}$ = rate of shear, sec^{-1}

τ = shear stress, dynes cm^{-2}

m = the consistency index, and

n = the flow-behavior index

Values for m and n were derived from the intercept and slope of the least-squares linear fit of log η to log $\dot{\gamma}$ for each experimental condition.

The power-law is the simplest and most widely used empirical model for non-Newtonian behavior (B2). Newtonian flow is characterized by a flow-behavior index of unity, whereas values less than one apply to pseudoplastic materials. This model fits the flow curves of many pseudoplastics over one or two decades of shear rate but does not apply to the extremes in shear rate because the equation predicts an infinite viscosity as the shear rate approaches zero and a zero viscosity for infinite shear rates.

The Ellis model was also used to describe the flow-behavior data in the form

$$\frac{1}{\eta} = \frac{1}{\eta_o}\left[1 + \left(\frac{\tau}{\tau_{1/2}}\right)^{\alpha-1}\right] \qquad [25]$$

where η_o = apparent viscosity at zero shear rate

$\tau_{1/2}$ = shear stress corresponding with 1/2 η_o

α = a parameter

This three-parameter model is more generally applicable to real fluids particularly at low shear rates because it describes a zero-shear viscosity, η_o. Since equation [25] is not suited to a direct solution, the parameters η_o, $\tau_{1/2}$ and α were evaluated using a trial-and-error computer method.

Temperature Effects on Flow Behavior

Temperature dependence of flow parameters

Flow-behavior parameters of polymer solutions have been shown to be dependent on temperature (T7), thus the power law and Ellis model parameters were examined as functions of temperature. The data were tested with several different functions and were found to be suitably described by equations similar to those of Turian (T7).

$$\log m = \log m^\circ + A\,\Theta \qquad [26]$$

$$n = n^\circ + B\,\Theta \qquad [27]$$

$$\log \eta_o = \log \eta_o^\circ + C\,\Theta \qquad [28]$$

$$\log \tau_{1/2} = \log \tau_{1/2}^\circ + D\,\Theta \qquad [29]$$

$$(1/\alpha) = (1/\alpha)^\circ + E\,\Theta \qquad [30]$$

where $\Theta = \frac{T - T^\circ}{T^\circ}$ [31]

T° = a reference temperature, 10°C

T = temperature, °C

A, B, C, D, and E are constants and the superscripted terms are values of the parameters at the reference temperature T°.

Temperature dependence of viscosity

Over a moderate range of temperatures the viscosity of most fluids changes according to the Arrhenius equation

$$\eta = Ae^{\Delta E/RT} \quad [32]$$

where A = a constant

ΔE = activation energy for viscous flow

R = gas constant

T = temperature, °K

Flow-behavior data were grouped according to shear rate and each set of data was fitted by equation [32] to evaluate A and ΔE.

Statistical Methods Used in Data Analysis

All rheological models were fitted to data by least-squares regression methods. Time-dependence tests each provided 30 observations whereas flow-behavior tests usually consisted of 24 separate measurements. In order to evaluate the effects of certain experimental conditions on viscous behavior, pairs of regressions were tested for differences of slope and level with a covariance analysis outlined by Snedecor (S7).

RESULTS AND DISCUSSION

Sample Quality

Average Haugh scores of 89.8 and 85.0 were obtained for twenty eggs from lots 1 and 2 respectively. The corresponding percentage solids were 12.92 and 11.36 and pH values during the tests were essentially constant at 8.4 $\pm$ 0.2. These data indicate that the albumen was of high quality; hence, some caution is recommended when estimating rheological properties of low quality albumen on the basis of the data reported herein. From the results of previous experiments at 2°C on egg albumen of high and low quality (T5), the effect of lower quality albumen would be more pronounced in the time-dependent characteristic than in the equilibrium flow-behavior.

Results of Time-Dependence Tests

Recovery of apparent viscosity after storage

In figure 20, the apparent-viscosity decay curve for three samples at 10°C and a shear rate of 3140 sec^{-1} is compared with the curve for tests repeated on the same samples 32 hours later. Since the two curves differ in slope and level ($P < 0.01$), albumen does not recover its original time-dependent characteristic. A criterion of thixotropy is that the material returns to its original structure when left undisturbed for a period of time following mechanical agitation. If structural breakdown is non-reversible, the fluid is said to

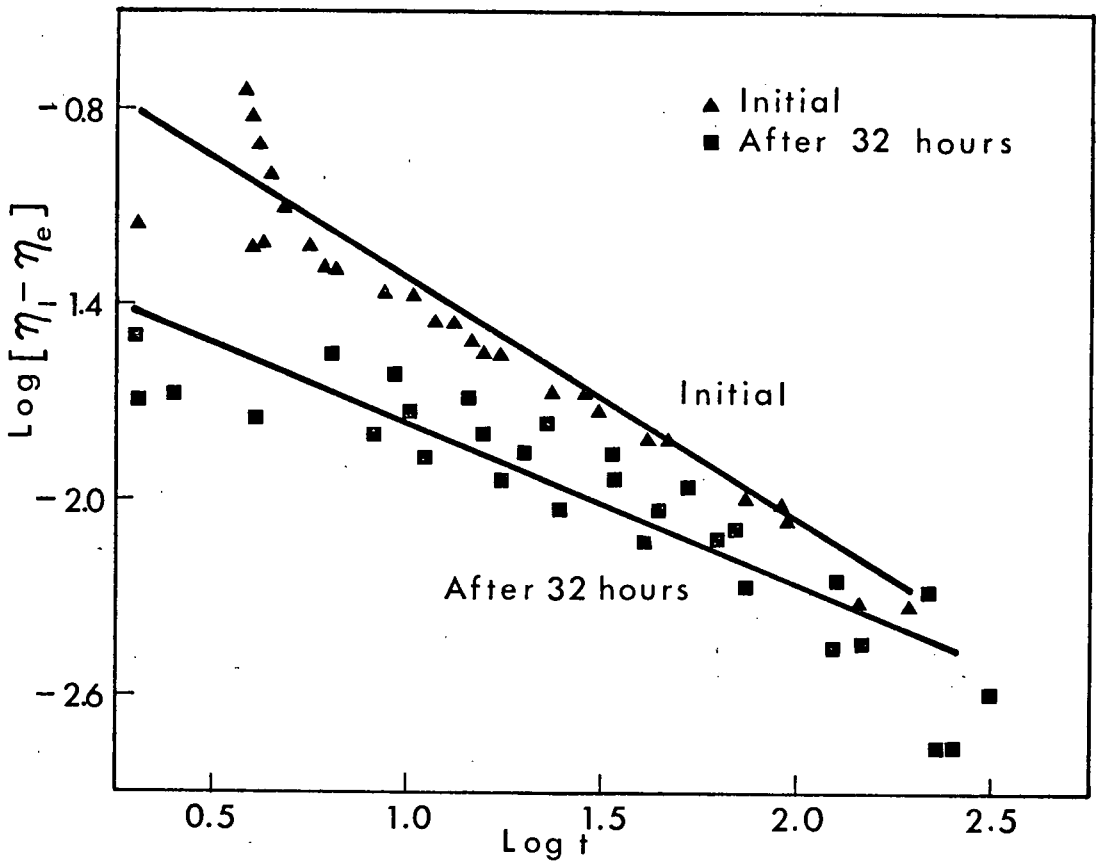

Figure 20. Apparent-viscosity decay in egg albumen tested before and after 32 hours storage. Tests at 10°C and 3140 sec^{-1} shear rate.

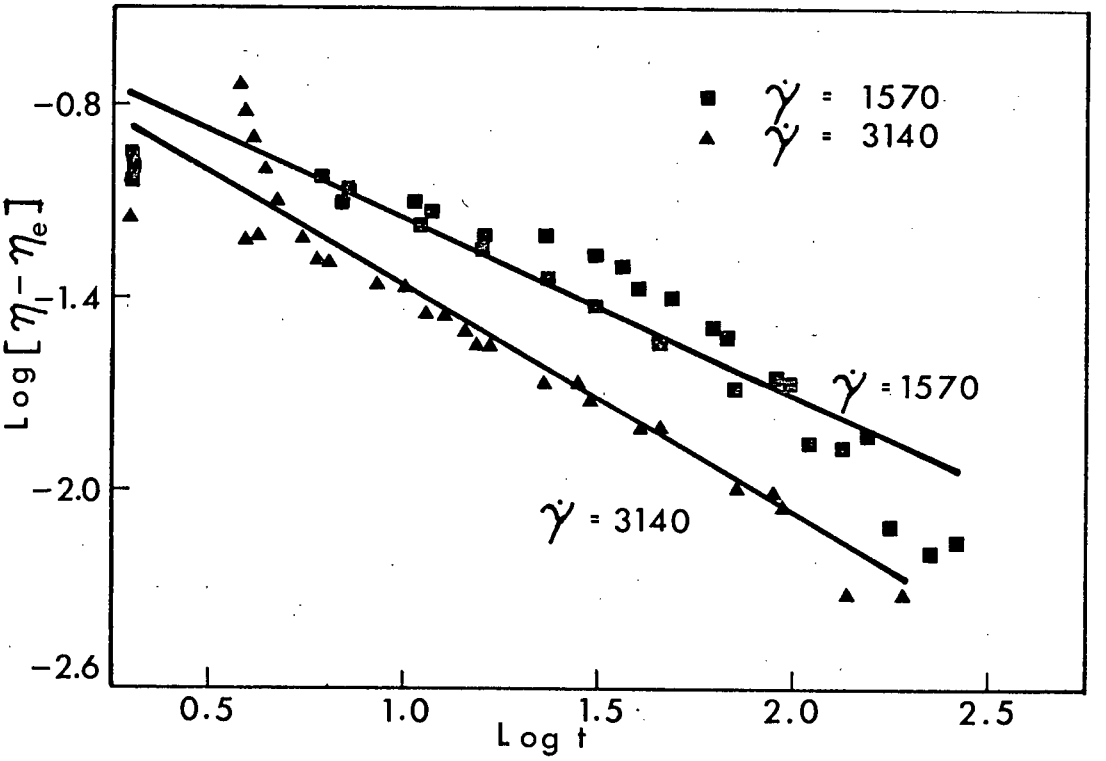

Figure 21. Apparent-viscosity decay in egg albumen at 10°C with shear rates of 1570 and 3140 sec^{-1}.

be rheodestructive (M2). There is, however, an appreciable recovery of structure because the apparent viscosity near the beginning of the second curve is much higher than the apparent viscosity of the initial curve at equilibrium. On the basis of these results, the structural breakdown mechanism in egg albumen at constant shear rate appears to be a combined thixotropic-rheodestructive process.

Effect of shear rate on apparent-viscosity decay

The effect of different shear rates on apparent-viscosity decay at 10°C is shown in figure 21 for shear rates of 1570 and 3140 sec^{-1}. Both the slope and level of the curves differ significantly ($P < 0.01$) with the more rapid decay and extensive breakdown at the higher shear rate. As a result of this observation, low shear rates are recommended for operations in which the viscous structure of albumen is to be preserved.

Effect of temperature on apparent-viscosity decay

Apparent-viscosity decay curves at 10, 20, 30 and 40°C are presented for the NV spindle (figure 22, Table XIII) and for the MV1 spindle (figure 23, Table XIV). It should be noted that data for the two spindles are considered separately because of their differing shear rates (for the NV spindle, $\dot{\gamma} = 3140\ sec^{-1}$ while for the MV1 spindle, $\dot{\gamma} = 1320\ sec^{-1}$). In covariance analyses of all possible pairs of lines from the two sets of data, the slopes are essentially the same

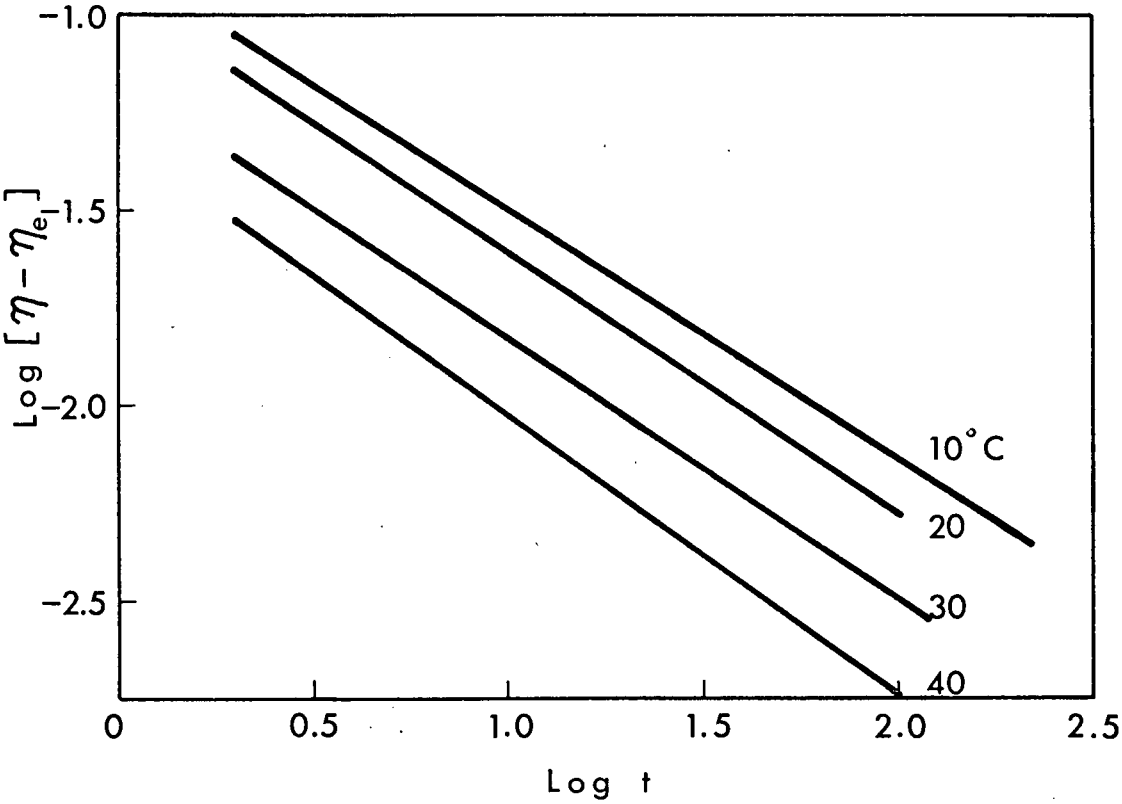

Figure 22. Apparent-viscosity decay curves at 10, 20, 30 and 40°C - NV spindle.

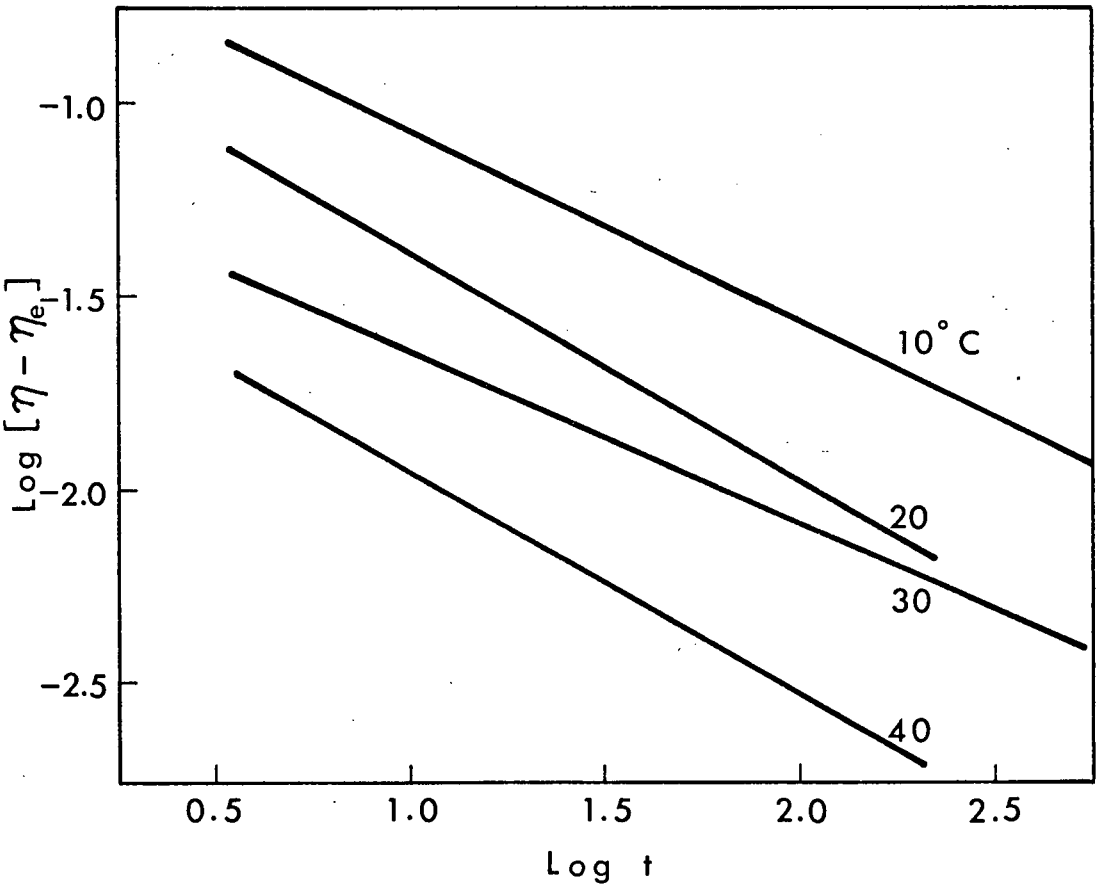

Figure 23. Apparent-viscosity decay curves at 10, 20, 30 and 40°C - MVI spindle.

TABLE XIII. APPARENT-VISCOSITY DECAY CURVES FOR NV SPINDLE

Temperature, °C	a_3†	b_3†	Sy††	r^2†††
10	1.138	-0.637	0.086	0.943
20	1.075	-0.676	0.089	0.939
30	0.827	-0.658	0.095	0.925
40	0.695	-0.715	0.082	0.949

† a_3, b_3 are constants defined by equation [22]

†† Standard error of estimate

††† Coefficient of determination (n = 30)

TABLE XIV. APPARENT-VISCOSITY DECAY CURVES FOR MV1 SPINDLE

Temperature, °C	a_3†	b_3†	Sy††	r^2†††
10	1.272	-0.439	0.166	0.790
20	1.027	-0.529	0.145	0.821
30	0.678	-0.399	0.232	0.531
40	0.457	-0.514	0.148	0.792

† a_3, b_3 are constants defined by equation [22]

†† Standard error of estimate

††† Coefficient of determination (n = 30)

($P > 0.05$) over the temperature range; however, the levels are significantly different ($P < 0.01$). That is, the rate of structural breakdown appears unaffected by temperature although viscosity is generally lower at higher temperatures.

Results of Flow-Behavior Tests

Effect of storage on flow-behavior

Power-law equations for the flow curves (figure 24) of the samples tested at 10°C before and after 32 hours of refrigerated storage are, respectively

$$\eta = 0.32\ \dot{\gamma}^{-0.24} \qquad [33]$$

$$\eta = 0.18\ \dot{\gamma}^{-0.18} \qquad [34]$$

The flow curves differ significantly ($P < 0.01$) in both slope and level, thus egg albumen appears to undergo a deterioration in viscous structure when tested and stored. Flow behavior indices (n) increase from 0.76 to 0.82 indicating that egg albumen becomes more Newtonian as a result of this treatment.

Effect of maximum shear rate on flow-behavior

Flow curves for samples tested with the NV spindle at 10°C, at maximum shear rates of 1570 and 3140 sec^{-1}, are shown in figure 25. The power-law equations for the data are

$$\eta = 0.32\ \dot{\gamma}^{-0.23} \qquad [35]$$

and

$$\eta = 0.32\ \dot{\gamma}^{-0.24} \qquad [36]$$

for maximum shear rates of 1570 and 3140 sec^{-1} respectively. Slopes of the two curves do not differ ($P > 0.05$); however, the levels are significantly different ($P < 0.01$). It should be noted that the flow curves are based on equilibrium apparent viscosities over a certain range of shear rates and

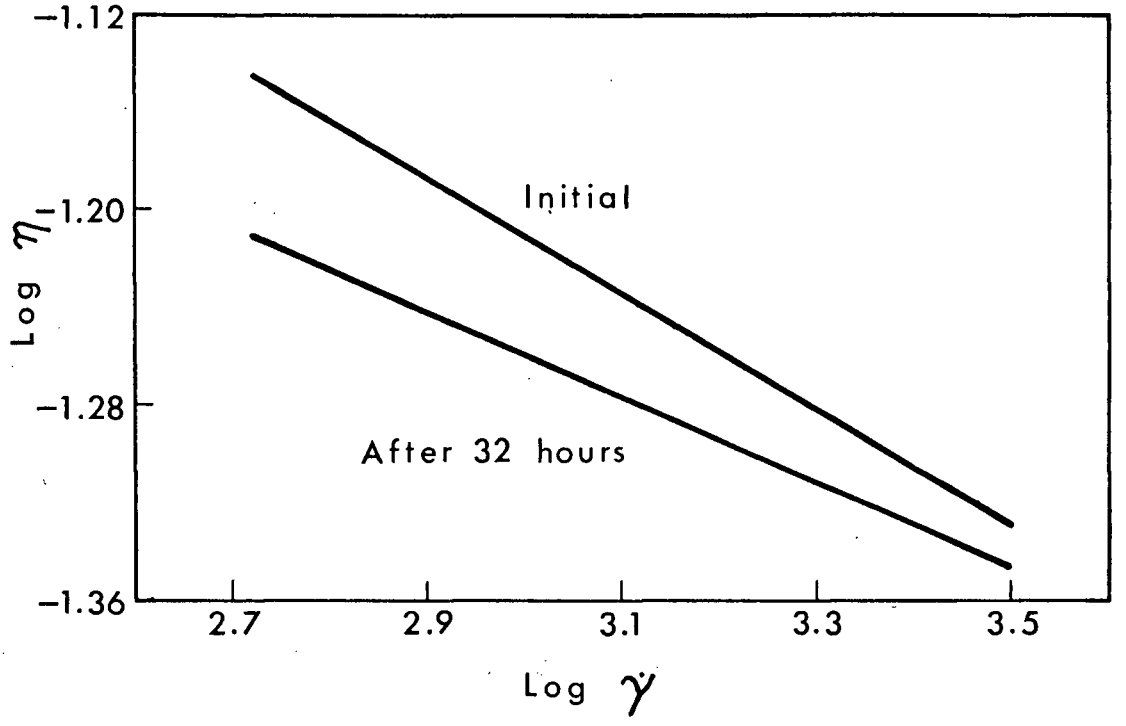

Figure 24. Flow behavior of egg albumen samples tested before and after 32 hours storage. Tests at 10°C with NV spindle.

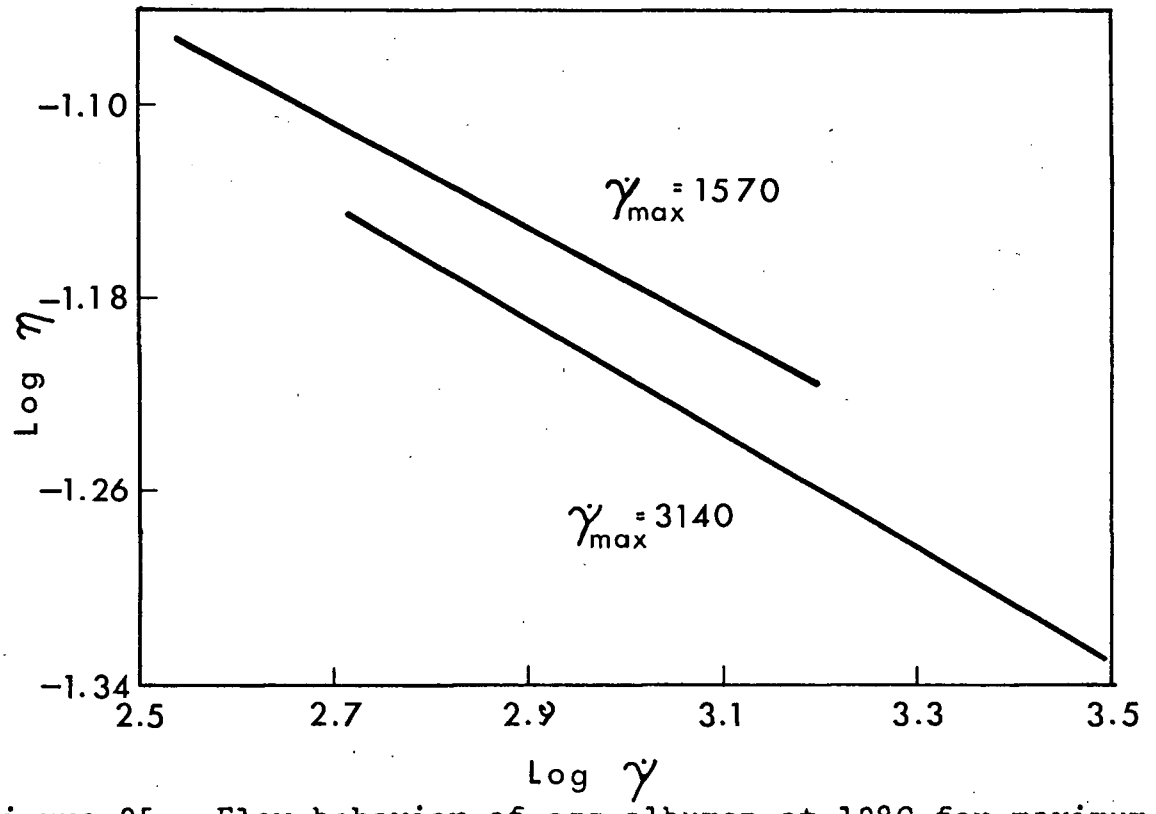

Figure 25. Flow behavior of egg albumen at 10°C for maximum shear rates of 1570 and 3140 sec^{-1}.

that the extent of structural breakdown in the fluid at a given temperature is determined by the maximum shear rate. Although most of the data for the two curves are within the same range of shear rates, the flow properties are quite different ($P < 0.01$). These results indicate that egg albumen rheology is strongly dependent upon the shear history of the fluid.

The power-law model of flow behavior

Power-law parameters for the albumen flow curves (figure 26) at 10, 20, 30 and 40°C are shown in Table XV for NV and MV1 spindles. For each of the four temperatures, flow curves obtained by the two spindles are significantly different ($P < 0.01$) thus, dependence of albumen flow behavior on shear history is confirmed. The average coefficient of determination of 0.762 for the eight curves indicates that the power-law accurately describes the flow behavior of egg albumen over the range of shear rates tested.

Covariance analyses of the six possible pairs of flow curves obtained from the NV-spindle show significant differences ($P < 0.05$) in slopes for all pairs except the 20-30°C and 30-40°C comparisons. All pairs of curves are significantly different ($P < 0.01$) in level. Thus, the flow curves for egg albumen between shear rates of 520 and 3140 sec^{-1} show some differences among flow-behavior indices and significant differences among apparent viscosities at ten degree intervals from 10 to 40°C. MV1-spindle results do not differ in slope ($P > 0.05$); however, all pairs of curves differ in level ($P < 0.01$) except for the 20-30°C lines.

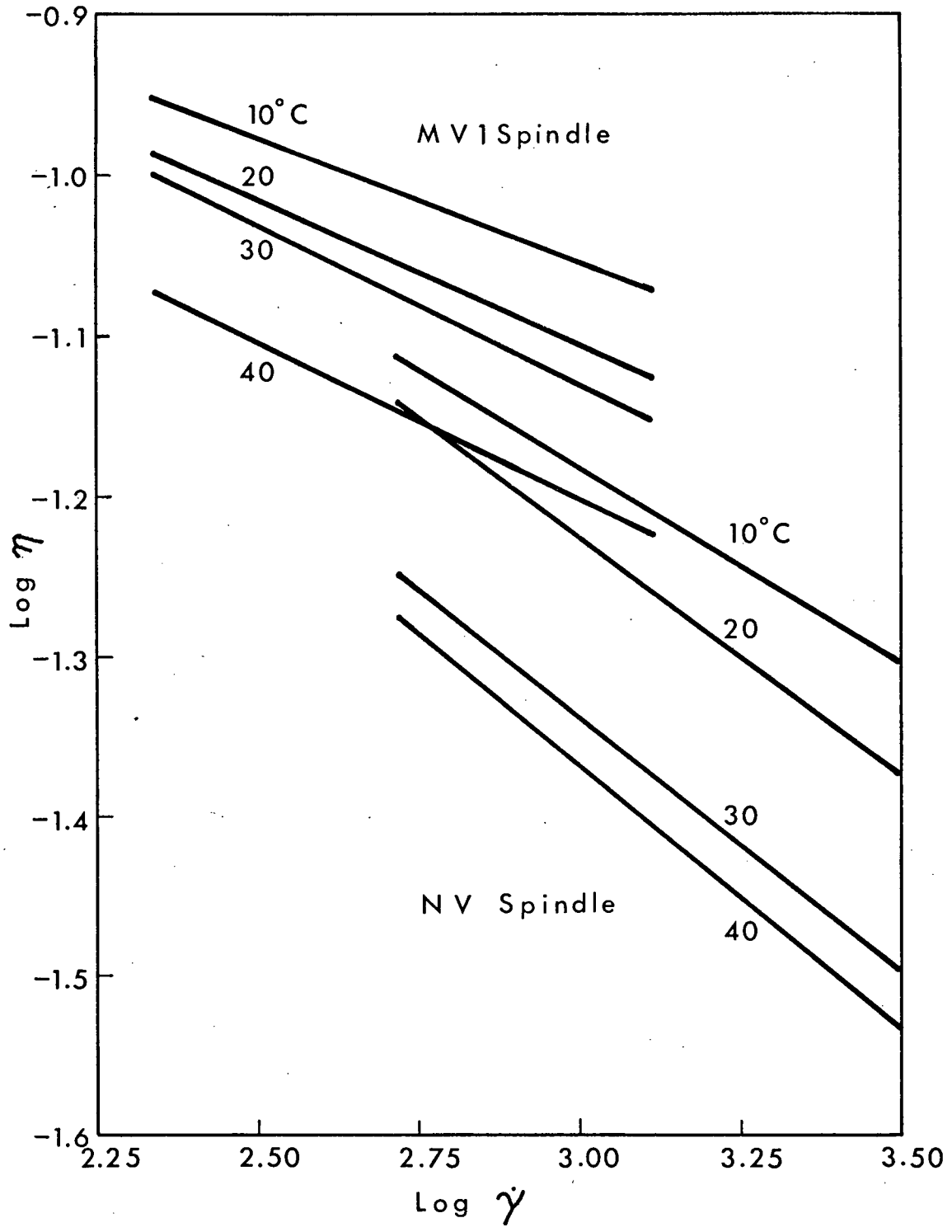

Figure 26. Flow-behavior curves for egg albumen at 10, 20, 30 and 40°C - NV and MVI spindles.

TABLE XV. POWER-LAW FLOW-BEHAVIOR CURVES FOR EGG ALBUMEN

Spindle	Temperature, °C	m	n	r^2†
NV††	10	0.351	0.757	0.798**
	20	0.457	0.704	0.760**
	30	0.433	0.674	0.942**
	40	0.424	0.667	0.897**
MVI†††	10	0.256	0.846	0.516**
	20	0.260	0.826	0.781**
	30	0.298	0.799	0.480**
	40	0.250	0.799	0.920**

† Coefficient of determination

†† Shear rates 520 - 3140 sec^{-1}

††† Shear rates 220 - 1320 sec^{-1}

** Significant at $P < 0.01$ with 22 degrees of freedom

It should be noted that for the NV-spindle tests, flow-behavior indices are smaller and show greater decreases per 10°C temperature rise than for the MVI-spindle tests. Experimental conditions for the two sets of tests are identical except that NV-spindle tests are at higher shear rates. Thus, for higher shear rates, egg albumen flow behavior becomes more pseudoplastic and furthermore shows greater pseudoplasticity per unit increase in temperature.

The Ellis model of flow behavior

Ellis model parameters for the flow behavior of egg albumen at 10, 20, 30 and 40°C are shown in Table XVI along with the coefficient of determination (r^2) for each condition. The average coefficient of determination (0.625) indicates that the Ellis model accurately ($P < 0.01$) describes albumen flow properties over the range of shear rates studied; however, the power-law provides a better fit of the data (average r^2 = 0.762). Because of lower accuracy of fit and relative difficulty in evaluating flow parameters, the Ellis model is not justified as a constitutive equation for egg albumen over the moderate range of shear rates studied.

Results for Temperature Effects on Flow Behavior

Effect of temperature on flow-behavior parameters

The power-law parameters for the flow curves of figure [26] vary with temperature as shown in figures [27] and [28]. Consistency coefficients (m) do not follow a clear trend; however, flow-behavior indices (n) steadily decrease

TABLE XVI. ELLIS MODEL FLOW-BEHAVIOR CURVES FOR EGG ALBUMEN

Spindle	Temperature	α	η_o	$\tau_{1/2}$	r^2†
NV††	10°C	1.51	0.124	78.4	0.765**
	20	1.72	0.121	56.2	0.725**
	30	1.76	0.086	51.1	0.928**
	40	1.82	0.081	47.8	0.844**
MVI†††	10	1.29	0.194	53.6	0.506**
	20	1.35	0.176	44.5	0.755**
	30	1.40	0.168	46.3	0.479**
	40	1.42	0.140	37.2	0.881**

† Coefficient of determination

†† Shear rates 520 - 3140 sec^{-1}

††† Shear rates 220 - 1320 sec^{-1}

** Significant at $P < 0.01$ with 22 degrees of freedom

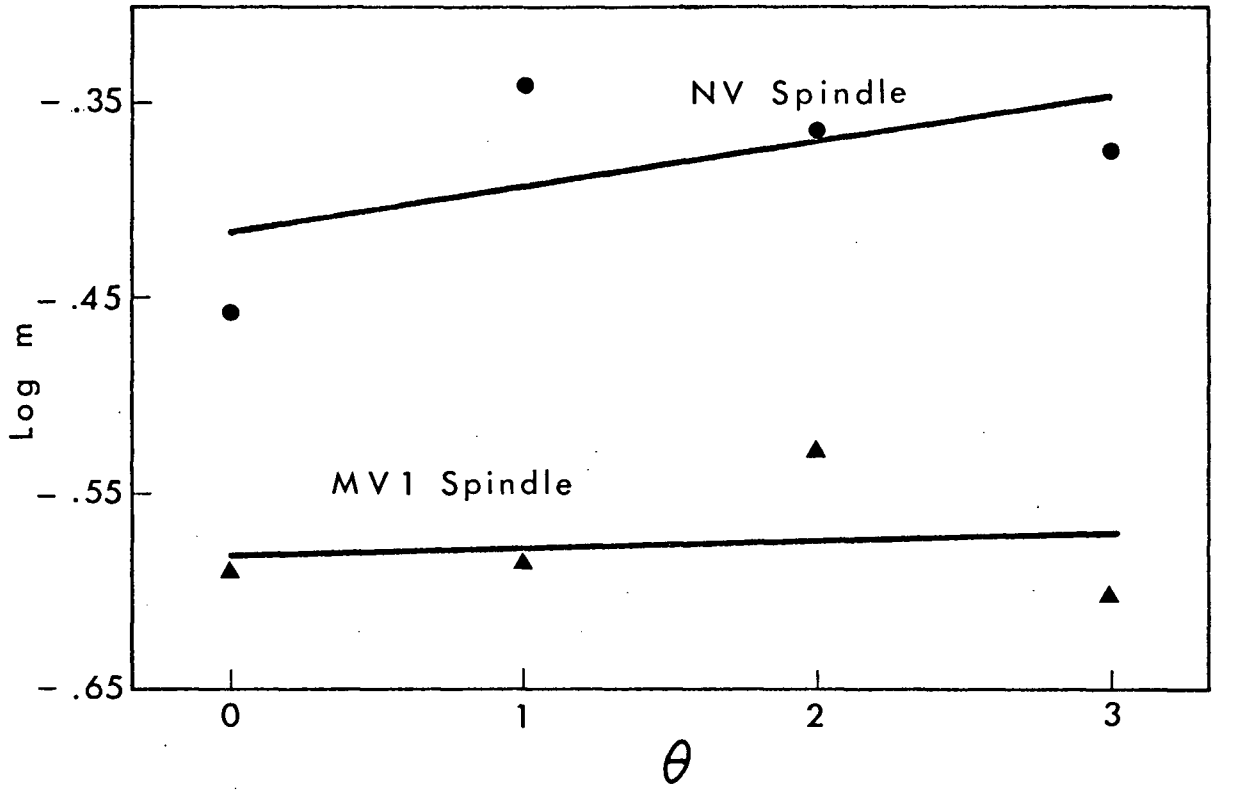

Figure 27. Temperature dependence of the power law parameter m.

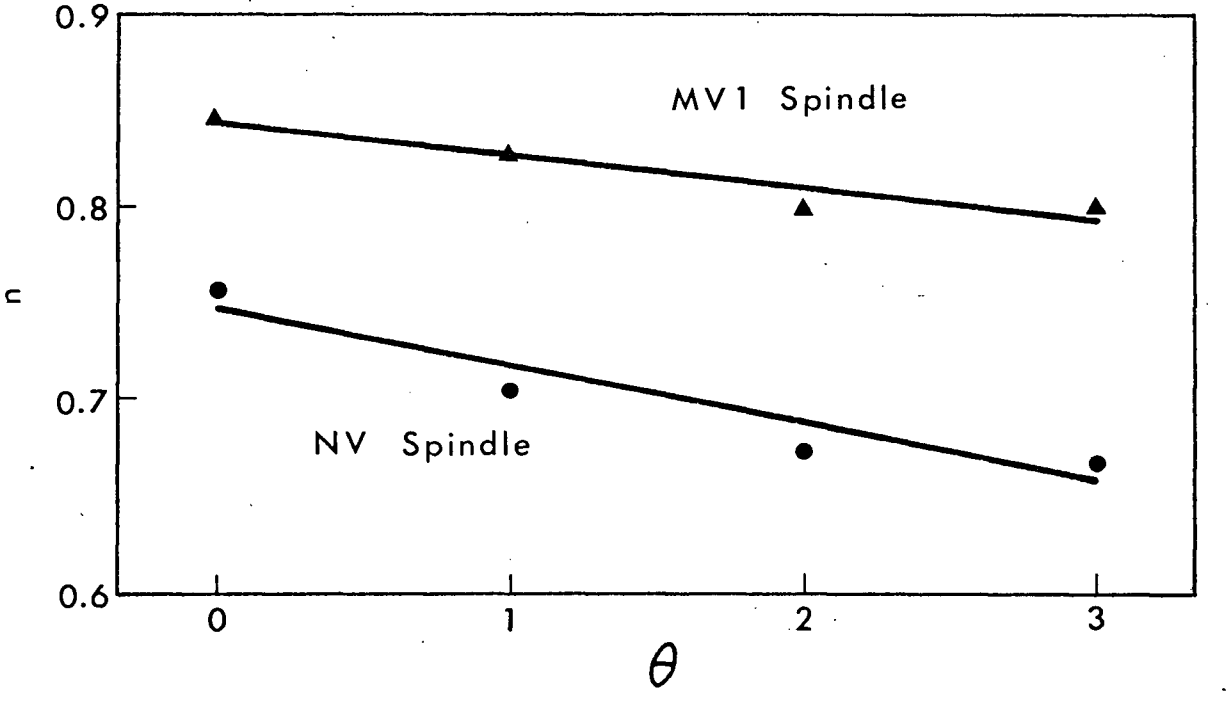

Figure 28. Temperature dependence of the power law parameter n.

with increasing temperature. Greater pseudoplasticity for higher temperatures indicates that egg albumen is more susceptible to structural breakdown at increased shear rates within the 220 to 3140 sec^{-1} range. As pointed out in an earlier discussion, smaller values of η° and B (Table XVII) for NV-spindle tests that for MVI-spindle tests, indicate that egg albumen flow behavior is more pseudoplastic and more sensitive to temperature changes at higher shear rates.

Variation of Ellis model parameters with temperature is shown in figures [29] to [31] with values of the constants in Table XVIII. Interpolation to evaluate flow parameters between 10 and 40°C is possible by means of these equations; however, these results are based on triplicate tests at only four temperatures and extrapolation beyond this range is not recommended.

Effect of temperature on apparent viscosity

Figures [32] and [33] show the temperature dependence of apparent viscosity using shear rate as a parameter. Activation energies for viscous flow of egg albumen (Table XIX) increase with shear rate and are consistently lower for the MVI-spindle data than for comparable shear rates with the NV spindle. A possible reason for this difference is the more extensive structural breakdown of albumen proteins when subjected to the higher maximum shear rates in the NV apparatus. Since the activation energy for viscous flow is a reflection of the attractions among particles in the fluid, higher values would be expected with the increased surface area of the disrupted protein molecules.

TABLE XVII. TEMPERATURE DEPENDENCE OF POWER-LAW FLOW-BEHAVIOR PARAMETERS

	NV Spindle	MVI Spindle
m°†	0.38	0.26
n°	0.75	0.84
A	0.023ns	0.0027ns
B	-0.030*	-0.017*

† Items in this column are defined in equations [26] and [27].

ns Not significant at $P < 0.10$.

* Significant at $P < 0.10$.

TABLE XVIII. TEMPERATURE DEPENDENCE OF ELLIS MODEL FLOW-BEHAVIOR PARAMETERS

	NV Spindle	MVI Spindle
η_o°†	0.13	0.19
$\tau^\circ_{1/2}$	73.0	53.0
$(1/\alpha)^\circ$	0.64	0.76
C	-0.070*	-0.043*
D	-0.069*	-0.046*
E	-0.035*	-0.022*

† Items in this column are defined in equations [28] to [30].

* Significant at $P < 0.10$.

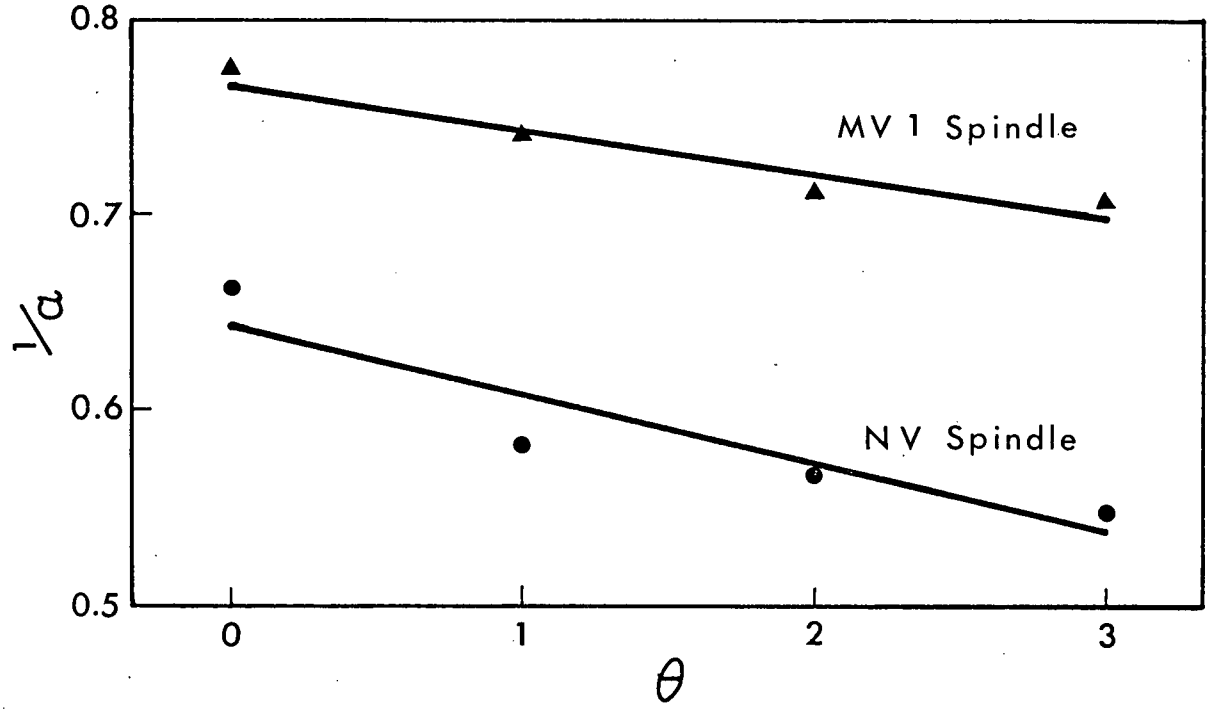

Figure 29. Temperature dependence of the Ellis parameter α.

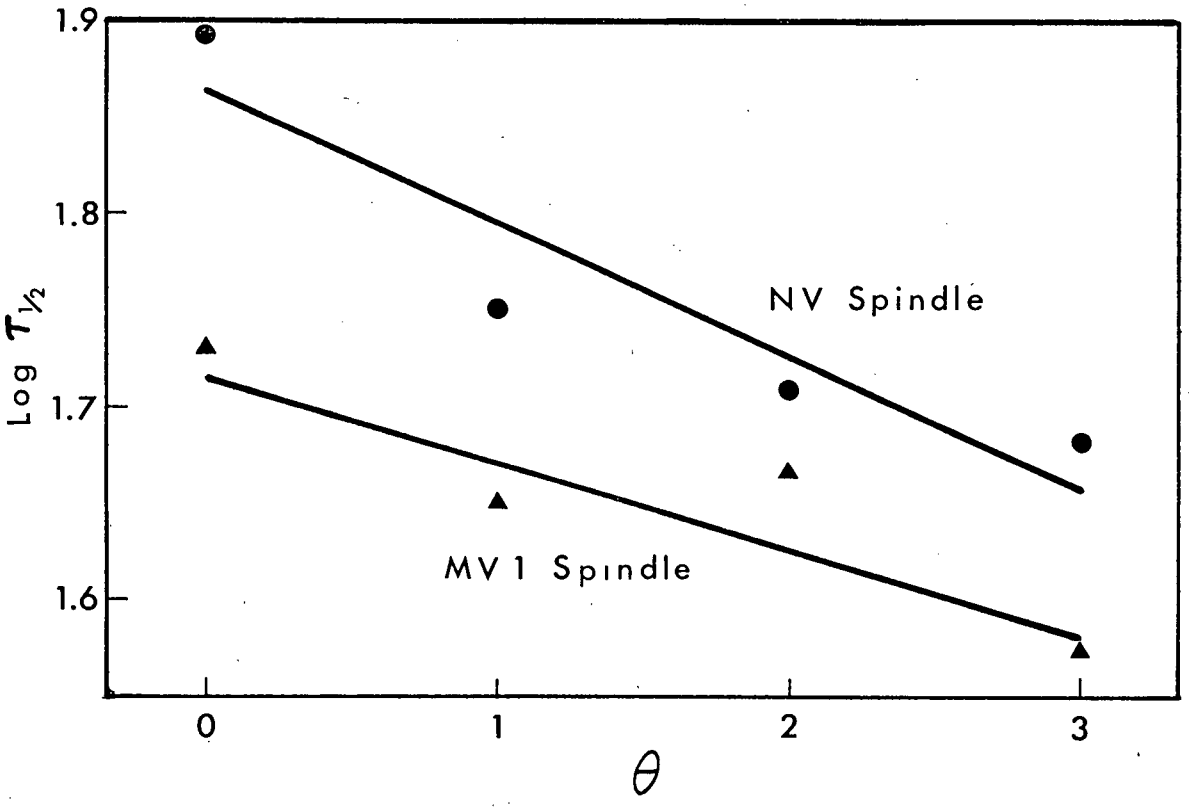

Figure 30. Temperature dependence of the Ellis parameter $\tau_{1/2}$.

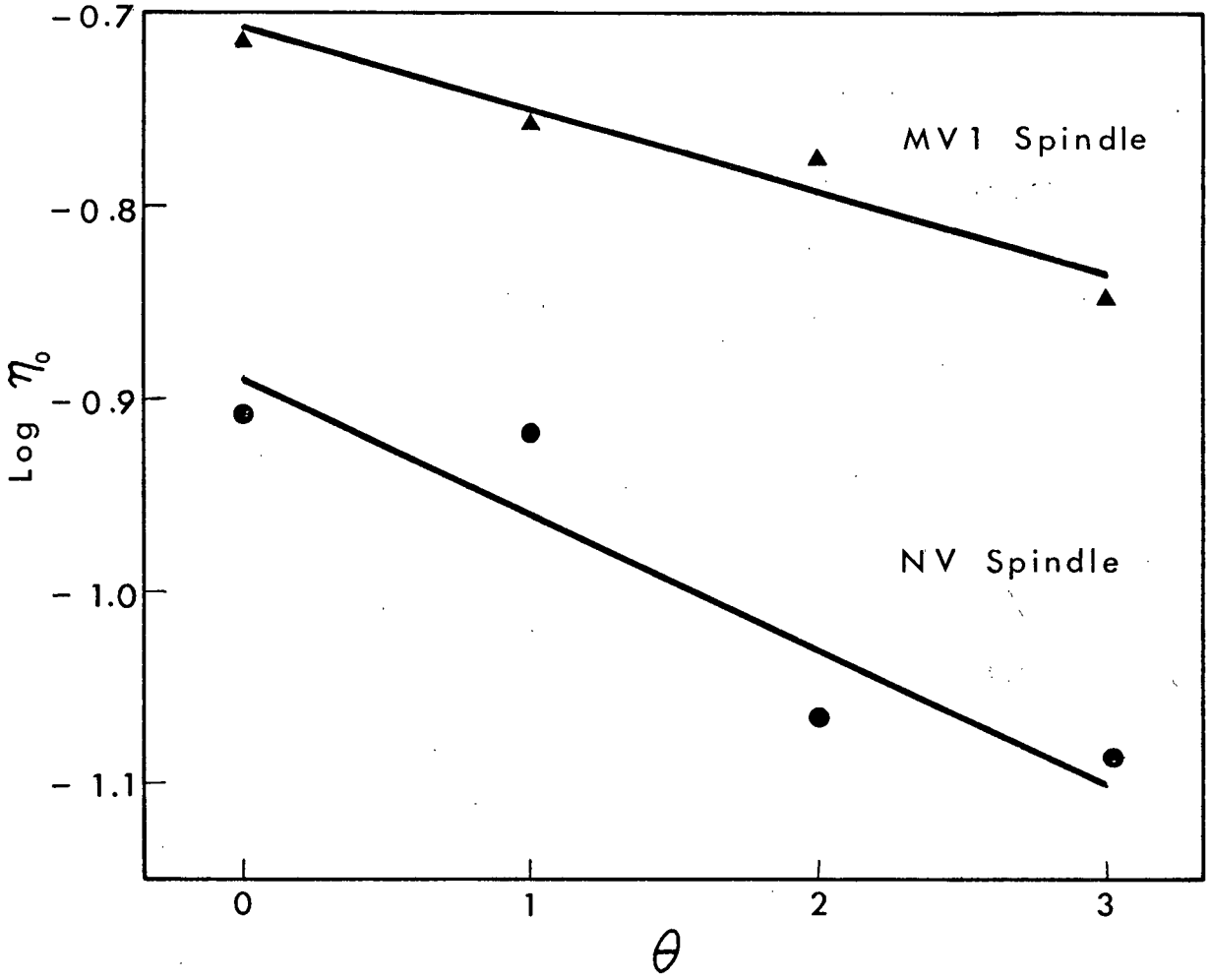

Figure 31. Temperature dependence of the Ellis parameter η_o.

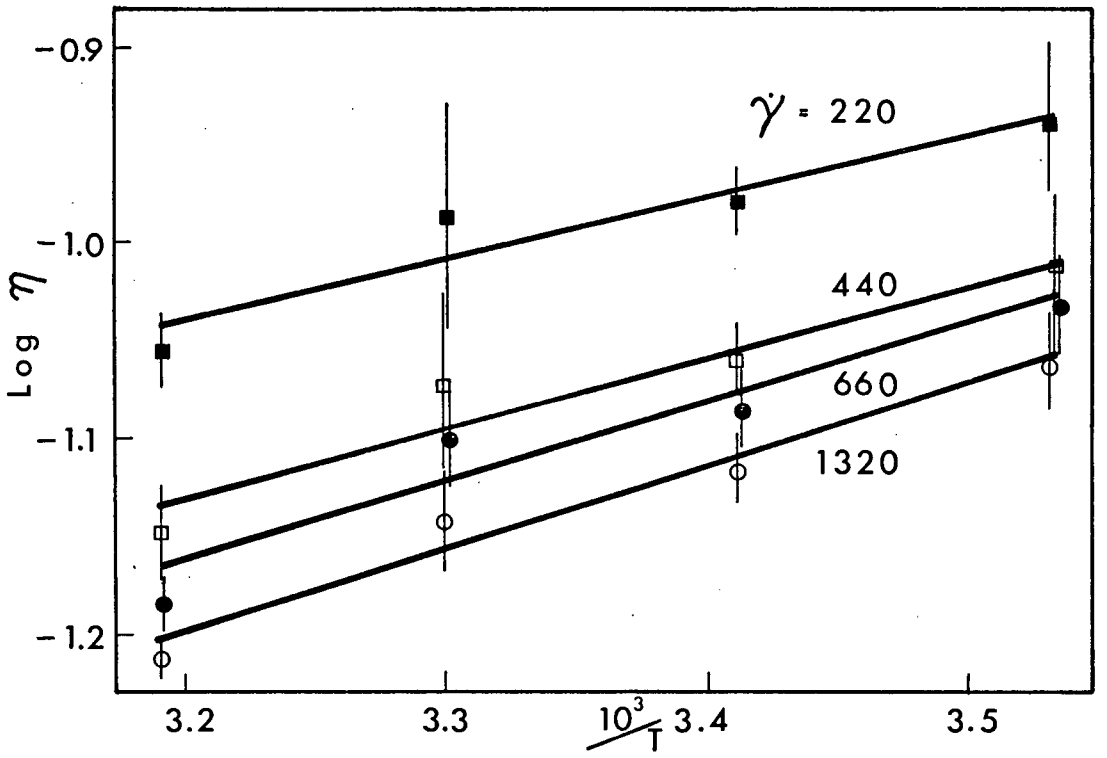

Figure 32. Temperature dependence of apparent viscosity using shear rate as a parameter - MV1 spindle.

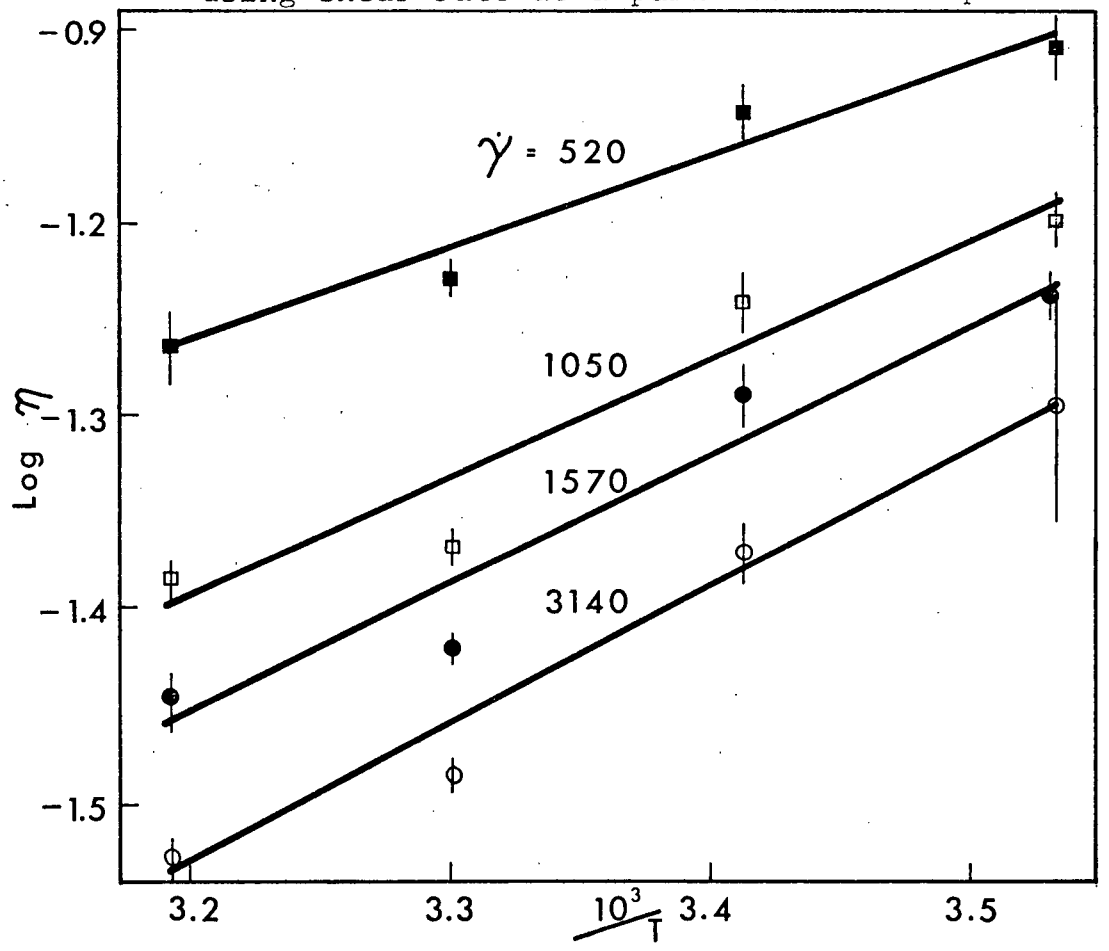

Figure 33. Temperature dependence of apparent viscosity using shear rate as a parameter - NV spindle.

TABLE XIX. TEMPERATURE DEPENDENCE OF APPARENT VISCOSITY USING SHEAR RATE AS A PARAMETER

Spindle	$\dot{\gamma}$	A†	ΔE††
NV	520	0.0015	22.5
	1050	0.00041	28.4
	1570	0.00024	30.8
	3140	0.00016	32.4
MVI	220	0.0091	14.3
	440	0.0049	16.8
	660	0.0032	19.0
	1320	0.0028	19.4

† Constant defined by equation [32]

†† Activation energy of viscous flow, kcal $mole^{-1}$

SUMMARY AND CONCLUSIONS

Rheological behavior of egg albumen was measured with a narrow-gapped concentric cylinder viscometer at temperatures of 10, 20, 30 and 40°C between shear rates of 220 to 3140 sec^{-1}. Apparent viscosity decreases with time at a constant rate of shear by a combined thixotropic-rheodestructive process. Temperature has little effect on the rate of structural breakdown although apparent viscosities decrease with increasing temperature. Higher shear rates result in a more rapid and extensive breakdown in egg albumen structure.

Egg albumen displays pseudoplastic flow behavior. Storage subsequent to testing, as well as the use of different maximum shear rates, results in different flow curves. The power-law and Ellis models accurately describe the flow data; however, the power-law is preferred because of a slightly better fit to the data over the range of shear rates studied. Flow-behavior parameters are temperature dependent and the apparent viscosity follows an Arrhenius relation for the temperatures tested. Activation energies of viscous flow vary from 14.3 to 32.4 kcal per mole under the conditions of this experiment.

LITERATURE CITED

A1 Atanasoff, J.V. and Wilcke, H.L. Measurement of the viscosity of eggs by the use of a torsion pendulum. J. Agr. Res. 54(9): 701-709, 1937.

B1 Ball, H.R. and Gardner, F.A. Physical and functional properties of gamma irradiated liquid egg white. Poultry Sci. 47(5): 1481-1487, 1968.

B2 Bird, R.B. Experimental tests of generalized Newtonian models containing a zero-shear viscosity and a characteristic time. Can. J. Chem. Eng., 161-168, August, 1965.

B3 Birks, L.S. Electron Probe Microanalysis. Interscience, New York, 1963.

B4 Boltz, D.F. Colorimetric Determination of Nonmetals. Interscience Publ., Inc., New York, 1958.

B5 Brant, A.W., Otte, A.W. and Norris, K.H. Recommended standards for scoring and measuring opened egg quality. Food Technol. 9: 356-361, 1951.

B6 Brooks, J. and Hale, H.P. Strength of the shell of the hen's egg. Nature 175: 848, 1955.

B7 Brooks, J. Strength in the egg. Soc. Chem. Ind. Mono. No. 7. Texture in Foods, London 149-178, 1958.

B8 Brown, L.C. and Thresh, H. Electron probe microanalysis. in Tools and Techniques in Physical Metallurgy. ed. Weinberg, F., Marcel Dekker Ltd., New York, 600-649, 1970.

B9 Brown, W.E., Baker, R.C. and Naylor, H.B. The role of the inner shell membrane in bacterial penetration of chicken eggs. Poultry Sci. 44(5): 1323-1327, 1965.

C1 Charm, S.E. Viscometry of non-Newtonian food materials. Food Res. 25(3): 351-362, 1960.

C2 Cramer, S.D. and Marchello, J.M. Procedure for fitting non-Newtonian viscosity data. AIChE J. 14(5): 814-815, 1968.

D1 Duncumb, P. and Reed, S.J.B. The calculation of stopping power and backscatter effects in electron probe microanalysis. in Quantitative Electron Probe Microanalysis. ed. Heinrich, K.F.J., N.B.S. Pub. No. 298, Washington, D.C. 133-154, 1968.

D2 Duncumb, P. and Shields, P.K. Effect of critical excitation potential on the absorption correction. in The Electron Microprobe. eds. McKinley, T.D., Heinrich, K.F.J. and Wittry, D.B., John Wiley and Sons, New York, 284-295, 1966.

E1 Elwell, W.T. and Gidley, J.A.F. Atomic Absorption Spectrophotometry. Pergamon Press, Oxford. 1966.

F1 Forsythe, R.H. The science and technology of egg products manufacture in the United States. in Egg Quality - A Study of the Hen's Egg. ed. Carter, T.C., Oliver and Boyd, Edinburgh, 1968.

G1 Garibaldi, J.A. and Stokes, J.L. Protective role of shell membranes in bacterial spoilage of eggs. Food Res. 23: 283-290, 1958.

G2 Goldstein, J.I. and Comella, P.A. A computer program for electron probe microanalysis in the fields of metallurgy and geology. Goddard Space Flight Center, Greenbelt, Maryland, 1969.

H1 Hahn, S.J., Ree, T. and Eyring, H. Flow mechanism of thixotropic substances. Ind. Eng. Chem. 51(7): 856-857, 1959.

H2 Hall, E.O. Variation of hardness of metals with grain size. Nature 173: 948, 1954.

H3 Hammerle, J.R. An engineering appraisal of egg shell strength evaluation techniques. Poultry Sci. 48(5): 1708-1717, 1969.

H4 Harper, J.C. and El Sahrigi, A.F. Viscometric behavior of tomato concentrates. J. Food Sci. 30(3): 470-476, 1965.

H5 Heinrich, K.F.J. X-ray absorption uncertainty. in The Electron Microprobe. eds. McKinley, T.D., Heinrich, K.F.J. and Wittry, D.B., John Wiley and Sons, New York, 296-377, 1966.

H6 Horowitz, W. ed. Official Methods of Analysis of the Association of Official Agricultural Chemists. 10th Ed., 257, 1965.

H7 Hunt, J.R. Distribution of magnesium in the egg shell. Poultry Sci. 47(5): 1683, 1968.

I1 Itoh, H. and Hatano, T. Variation of magnesium and phosphorus deposition rates during egg shell formation Poultry Sci. 43(1): 77, 1964.

K1 Kaufman, V.F., Ijichi, K. and Putnam, G.W. Flow characteristics in holding tubes of commercial egg pasteurizers. J. Milk and Food Technol. 31: 269-273, 1968.

K2 Keil, K. The electron microprobe X-ray analyzer and its application in mineralogy. Fortschr. Miner. 44(1): 4-66, 1967.

L1 Lifshitz, A., Baker, R.C. and Naylor, H.B. The relative importance of chicken egg exterior structures in resisting bacterial penetration. J. Food Sci. 29(1): 94-99, 1964.

L2 Longree, K., Beaver, S., Buck, P. and Nowrey, J.E. Viscous behavior of custard systems. J. Agr. Food Chem. 14(6): 653-659, 1966.

L3 Luft, J.H. Improvements in epoxy-resin embedding methods. J. Biophys. Biochem. Cytol. 9: 409, 1961.

M1 Masshoff, W. and Stolpmann, H.J. Licht und elektronenmikroskopische untersuchungen an der schalenhaut und kalkschale des hühnereies. Z. Zellforsch. 55: 818-832, 1961.

M2 Moses, G. and Vamos, E. Generalized Newtonian fluids and structural viscosity. Thixotropic phenomena. Int. Chem. Eng. 6(1): 150-159, 1966.

M3 Mott, B.W. Microindentation Hardness Testing. Butterworth's Scientific Publications, London, 1956.

N1 Nathusius, W.V. Avian Eggshells. ed. and trans. Tyler, C., Berkshire Printing, Reading, 1964.

O1 Ogilvie, R.E. Quantitative electron microprobe analysis. in Progress in Analytical Chemistry, Vol. I X-Ray and Electron Methods of Analysis. eds. Van Olphen, H. and Parrish, W., Plenum Press, New York, 55-75, 1968.

P1 Philibert, J. Method of calculating the absorption correction in electron-probe microanalysis. in X-Ray Optics and X-Ray Microanalysis - 3rd Symposium. eds. Prattee, H.H., Cosslett, V.E. and Engstrom, A., Academic Press, New York, pp. 379-392, 1963.

R1 Reed, S.J.B. Characteristic fluorescence corrections in electron-probe microanalysis. Brit. J. Appl. Phys. 16: 913-926, 1965.

R2 Reynolds, E.S. The use of lead citrate at high pH as an electron-opaque stain in electron microscopy. J. Cell Biol. 17: 208-212, 1963.

R3 Romanoff, A.L. and Romanoff, A.J. The Avian Egg, Chapman and Hall, London, 1949.

R4 Rowan, J.D., Norris, K.H. and Powell, C.K. A method for measuring rheological properties of eggs. Food Res. 23(6): 670-675, 1958.

S1 Saravacos, G.D. Effect of temperature on viscosity of fruit juices and purees. J. Food Sci. 35(2): 122-125, 1970.

S2 Simkiss, K. The structure and formation of the shell and shell membranes. in Egg Quality - A Study of the Hen's Egg. ed. Carter, T.C., Oliver and Boyd, Edinburgh, 1968.

S3 Simkiss, K. and Tyler, C. A histochemical study of the organic matrix of hen egg-shells. Quart. J. Micr. Sci., 98(1): 19-28, 1957.

S4 Simons, P.C.M. and Wiertz, G. Notes on the structure of membranes and shell in the hen's egg. An electron microscopical study. Zeits. für Zellfors. 59: 555-567, 1963.

S5 Smith, A.J.M. Viscosity of the white and of the yolk. Rep. Food Inv. Bd., 53-56, 1934.

S6 Smith, J.V. X-ray emission microanalysis of rock-forming minerals. I. Experimental techniques. J. Geol. 73: 830-864, 1965.

S7 Snedecor, G.W. Statistical Methods. 5th Ed. Iowa State Univ. Press, Ames, Iowa, 1956.

S8 Stewart, G.F. The structure of the hen's egg shell. Poultry Sci. 14: 24-32, 1935.

T1 Tabor, D. The physical meaning of indentation and scratch hardness. Br. J. Appl. Phys. 7: 159, 1956.

T2 Terepka, A.R. Structure and calcification in avian egg shell. Exptl. Cell Res. 30: 171-182, 1963.

T3 Tung, M.A. Studies on physical properties of egg shells. Unpublished M.S.A. Thesis. University of British Columbia, 1967.

T4 Tung, M.A., Staley, L.M. and Richards, J.F. Studies on hardness of the hen's egg shell. J. Agric. Eng. Res. 13(1): 12-18, 1968.

T5 Tung, M.A., Richards, J.F., Morrison, B.C. and Watson, E.L. Rheology of fresh, aged and gamma-irradiated egg white. J. Food Sci. (in press) 1970.

T6 Tung, M.A., Staley, L.M. and Richards, J.F. The relation of chemical composition to hardness in the hen's egg shell. Paper presented at the 1969 Annual Meeting, Can. Soc. Agr. Eng., Saskatoon, Sask., (August 24-28, 1969).

T7 Turian, R.M. Thermal phenomena and non-Newtonian viscometry. Ph.D. Thesis, Univ. of Wisconsin, 1964.

T8 Tyler, C. and Geake, F.H. Studies on egg shells. XV - Critical appraisal of various methods of assessing shell thickness. J. Sci. Food Agric. 12: 281-289, 1961.

T9 Tyler, C. Shell strength: Its measurement and relationship to other factors. Brit. Poultry Sci. 2: 3-19, 1961.

V1 Van Wazer, J.R., Lyons, J.W., Kim, K.Y. and Colwell, R.E. Viscosity and Flow Measurement, Interscience, New York, 1963.

W1 Walden, C.C., Allen, I.V.F. and Trussell, P.C. The role of the egg shell and shell membranes in restraining the entry of microorganisms. Poultry Sci. 35: 1190-1196, 1956.

W2 Watson, E.L. Rheological behavior of apricot purees and concentrates. Can. Agr. Eng. 10(1): 8-11, 1968.

W3 Wells, R.G. The measurement of certain egg quality characteristics: A review. in Egg Quality - A Study of the Hen's Egg. ed. Carter, T.C., Oliver and Boyd, Edinburgh, 1968.

W4 Weltman, R.N. Breakdown of thixotropic structure as a function of time. J. Appl. Phys. 14: 343-350, 1943.